A multi-year study of lower tropospheric aerosol variability and systematic relationships from four North American regions

J.P. Sherman[1], P.J. Sheridan[2], J.A. Ogren[2], E. Andrews[3], D. Hageman[3], L. Schmeisser[3], A. Jefferson[3], and S. Sharma[4]

[1] {Dept. Physics and Astronomy, Appalachian State University, 525 Rivers St, CAP Building, Room 231, Boone, NC, USA 28608}

[2] {NOAA, Earth Systems Research Laboratory, Global Monitoring Division/GMD-1, 325 Broadway, Boulder, CO USA 80305}

[3] {CIRES, University of Colorado, Boulder, Colorado, 80309}

[4] {Environment Canada, 4905 Dufferin St, Toronto, ON, M3H 5T4 Canada}

Correspondence to: J.P. Sherman (shermanjp@appstate.edu)

Abstract

Hourly-averaged aerosol optical properties (AOPs) measured over the years 2010-2013 at four continental North American NOAA Earth System Research Laboratory (NOAA/ESRL) cooperative aerosol network sites – Southern Great Plains near Lamont, OK (SGP), Bondville, IL (BND), Appalachian State University in Boone, NC (APP), and Egbert, Ontario, Canada (EGB) are analyzed. Aerosol optical properties measured over 1996-2009 at BND and 1997-2009 at SGP are also presented. The aerosol sources and types in the four regions differ enough so as to collectively represent rural, anthropogenically-perturbed air conditions over much of eastern continental North America. Temporal AOP variability on monthly, weekly, and diurnal timescales is presented for each site. Differences in annually-averaged AOPs and those for individual months at the four sites are used to examine regional AOP variability. Temporal and regional variability are placed in the context of reported aerosol chemistry at the sites, meteorological measurements (wind direction, temperature), and reported regional mixing layer heights. Basic trend analysis is conducted for selected AOPs at the long-term sites (BND and SGP). Systematic relationships among AOPs are also presented.

Seasonal variability in PM1 (sub-1μm particulate matter) scattering and absorption coefficients at 550 nm (σ_{sp} and σ_{ap}, respectively) and most of the other PM1 AOPs is much larger than day of week and diurnal variability at all sites. All sites demonstrate summer σ_{sp} and σ_{ap} peaks. Scattering coefficient decreases by a factor of 2-4 in September-October and coincides with minimum single-scattering albedo (ω_0) and maximum hemispheric backscatter fraction (b). The co-variation of ω_0 and b lead to insignificant annual cycles in top-of-atmosphere direct radiative forcing efficiency (DRFE) at APP and SGP. Much larger annual DRFE cycle amplitudes are observed at EGB (~40%) and BND (~25%), with least negative DRFE in September-October at both sites. Secondary winter peaks in σ_{sp} are observed at all sites except APP. Amplitudes of diurnal and weekly cycles in σ_{ap} at the sites are larger for all seasons than those of σ_{sp}, with largest differences occurring in summer. The weekly and diurnal cycle amplitudes of most intensive AOPs (e.g., those derived from ratios of measured σ_{sp} and σ_{ap}) are minimal in most cases, especially those related to parameterizations of aerosol size distribution.

Statistically significant trends in σ_{sp} (decreasing), PM1 scattering fraction (decreasing), and b (increasing) are found at BND from 1996-2013 and at SGP from 1997-2013. A statistically significant decreasing trend in PM10 scattering Ångström exponent is also observed for SGP but not BND. Most systematic relationships among AOPs are similar for the four sites and are adequately described for individual seasons by annually-averaged relationships, although relationships involving absorption Ångström exponent vary with site and season.

1 Introduction

Predictions of future climate change resulting from projected increases in carbon dioxide are limited by large uncertainties in the direct and indirect radiative forcing due to aerosols (Andreae et al., 2005). Measurement-based estimates of globally-averaged aerosol direct radiative forcing (DRF) are 55-80% greater than the model-based estimates (Yu et al., 2009). The measurement-model differences are even larger on regional scales and for the anthropogenic component (Yu et al., 2009). Such measurement-model discrepancies are the result of a combination of differences in aerosol amount, single-scattering albedo, surface albedo, and radiative transfer schemes (Yu et al., 2006). One of the high-priority tasks recommended to reduce the uncertainty in aerosol radiative effects is to "*Maintain,*

enhance, and expand the surface observation networks measuring aerosol optical properties for satellite retrieval validation, model evaluation, and climate change assessments" (Kahn et al., 2009).

Studies based on long-term measurements made by global surface-based aerosol monitoring networks such as NASA's Aerosol Robotic Network (AERONET) and NOAA's Earth System Research Laboratory (NOAA/ESRL) have contributed to improved understanding of mean values of aerosol optical properties (AOPs), spatial and temporal AOP variability, and relationships among some AOPs (Dubovik et al., 2005; Delene and Ogren, 2002; hereafter referred to as D&O2002). The US-based Interagency Monitoring of Protected Visual Environments (IMPROVE) network (Malm et al., 2004) has conducted similar studies using speciated aerosol mass concentrations, aerosol light scattering coefficient (at some sites), and reconstructed aerosol light extinction coefficient measurements in remote areas of the US. Recent long-term trend studies based on data from surface networks indicated that aerosol optical depth (Li et al., 2014; Yoon, 2012) and lower tropospheric aerosol light scattering coefficient (Collaud-Coen et al., 2013; hereafter referred to as CC2013) decreased at a majority of North American aerosol monitoring sites. Hand et al. (2014) reported large reductions of up to 50% in reconstructed aerosol visible light extinction for the 20% haziest days annually at IMPROVE sites in the US from 2002-2011, with the largest decreases in the eastern US. Through trend analysis of speciated aerosol mass concentrations and emissions inventories, Hand et al. (2014) showed that reductions in US SO_2 emissions have likely played a major role in the reduced aerosol light extinction, particularly in the eastern US. Murphy et al. (2011) applied trend analysis to data from IMPROVE sites across the US to show that elemental carbon aerosol mass concentrations decreased by over 25% between 1990-2004, with reductions during winter months close to 50%. Region- and season-dependent changes in emissions of aerosols and precursor gases may result in changes in mean values and variability of aerosol optical and microphysical properties. However, few long-term studies of aerosol intensive properties (e.g., properties that are independent of aerosol loading, such as single scattering albedo, asymmetry parameter, and direct radiative forcing efficiency) have been conducted in or over multiple North American regions.

Surface-based networks employing in situ measurements of aerosol optical properties,

such as the WMO Global Atmosphere Watch (GAW) and NOAA/ESRL aerosol networks are particularly well- suited for studies of aerosol variability on a variety of temporal scales under both clear and cloudy conditions. An additional advantage of the in situ measurements is the ability to derive single-scattering albedo under low aerosol loading conditions. Column-averaged single scattering albedo derived from sky radiance measurements made by Cimel sun/sky radiometers as part of AERONET possess high uncertainties at the lower aerosol optical depths (AOD) typical of most rural North American sites (Dubovik et al., 2000). A weakness of many in situ surface aerosol measurement systems is the inability to determine the hygroscopic dependence of aerosol light scattering. Many aerosol monitoring stations in the NOAA/ESRL and GAW networks follow similar sampling protocols where the aerosols are dried to decouple the aerosol properties from local variations in relative humidity (RH). Another concern is the uncertainty as to when and under what conditions the near-surface measurements are representative of the atmospheric column at each site. The first problem can be addressed through the use of humidified light scattering measurements (e.g., Sheridan et al., 2001), which are or have been made at a few ESRL network sites, including three of the four sites reported in this paper. The second issue has been investigated through multi-year aircraft measurement programs over instrumented surface sites. At the Southern Great Plains (near Lamont, OK) and Bondville, IL sites respectively, Andrews et al. (2004) and Sheridan et al. (2012) reported that median values of key low-RH intensive AOPs exhibited little statistical variability up to ~2 km altitude and that long-term median values could be well-approximated by the near-surface values. Instantaneous measurements of the near-surface properties were often poorly-correlated with those of the column at these sites. (Andrews et al., 2004; Sheridan et al., 2012).

D&O2002 reported multi-year measurements of AOPs at four North American sites that were used to (1) highlight the need to quantify both aerosol extensive properties (e.g., properties that depend on aerosol amount) and aerosol intensive properties on regional scales over at least a 1-year period; and (2) conclude that global AOD measurements made daily by satellites, combined with in situ measurements of regionally-representative intensive AOPs, are likely sufficient to determine aerosol DRF with a relatively small amount of uncertainty. One limitation of their study was the then-lack of NOAA/ ESRL network

sites in the more populous eastern continental North America. D&O2002 also studied systematic relationships between aerosol loading (using scattering coefficient as a proxy) and other AOPs. D&O2002 argued the importance of such relationships for applications including inversion of remote sensing data, whereby a dynamic model could be used to specify the constraining AOPs as a function of aerosol loading.

The study described here utilizes four years (2010-2013) of continuous measurements of aerosol light absorption, scattering, and hemispheric backscattering coefficients made at four continental North American sites (Fig. 1; Table 1) in the NOAA/ESRL cooperative aerosol network: (i) the Appalachian Atmospheric Interdisciplinary Research facility at Appalachian State University (APP) in Boone, NC- located in the southern Appalachian mountain region of the southeastern US.; (ii) the Bondville Environmental and Atmospheric Research Site (BND), located in the agricultural Midwestern US near Champaign, IL; (iii) the Environment Canada monitoring station at Egbert, Ontario (EGB) - located in the agricultural and forested rural region north/ northwest of Toronto; and (iv) the Southern Great Plains Central Facility (SGP) of the US Department of Energy Atmospheric Radiation Measurement program (SGP), located in the southern plains of the US in rural Oklahoma. We use these measurements to calculate several key AOPs relevant to aerosol radiative forcing (Table 2). Hourly-averaged AOPs are binned by month, day of week, and hour of day to study annual, weekly, and diurnal AOP cycles at each site. AOPs are also binned by wind sector for each season to study the role of known regional aerosol sources on AOPs and their variability at each site. Published aerosol chemistry for each site and its seasonal variability are used along with published mixing layer heights for each region and monthly median temperatures at the sites to help explain the AOP cycles at each site and differences among sites. Basic trend analysis is conducted for selected AOPs at the long-term sites (BND and SGP). Systematic relationships among AOPs are also presented. The objectives are to

(1) provide an explanation of temporal and regional AOP variability that is consistent with meteorology, regional aerosol sources, and reported aerosol chemistry at the sites;

(2) identify possible AOP trends at the long-term sites (SGP and BND);

(3) determine whether systematic relationships exist for key aerosol properties relevant to aerosol DRF calculations.

In addition to our use of meteorology and published aerosol chemistry to interpret the AOP

variability, this study differs from the D&O2002 paper in three respects:

(1) The time period of the study is different, which allows for us to compare (at least for BND and SGP) how the AOPs have changed in the intervening years;

(2) This paper has a focus on continental sites, whereas D&O2002's four sites included an Arctic site and a marine site;

(3) We report the following for individual seasons: (a) diurnal and weekly AOP variability, and (b) some systematic relationships involving aerosol absorption Ångström exponent. D&O2002 reported select AOPs for full years.

2 Methodology

2.1 Air sampling infrastructure at the sites

The APP, BND, EGB, and SGP sites are all designed with similar inlet systems following established NOAA/ESRL and GAW aerosol sampling protocols (e.g., Sheridan et al., 2001; WMO, 2003). To minimize contamination from local activities around the stations, ambient aerosols are sampled from the top of sampling stacks that are well above the surrounding terrain. The top of the stack is 10 m above the ground at BND, EGB, and SGP. The sampling inlet at APP is located at the top of a 34 m tall tower in order to sample aerosols at a height > 5 m above the surrounding tree canopy. To reduce the confounding effects of relative humidity (RH) on the aerosol measurements, the sample air is gently heated when needed at all sites except EGB to achieve sample line and instrument RH ≤ 40% (Sheridan et al., 2001). Nephelometer instrument RH at EGB exceeds 40% for a majority of hours in July-September but the moderately-elevated instrument RH during these months is not believed to have any substantial impact on the results presented in this paper (Sect. S3 of Supplementary Materials).

All of the sites except EGB use a switched impactor system (e.g., Sheridan et al., 2001) to alternate between sub-10μm (D_p < 10 μm) and sub-1μm (D_p < 1 μm) aerodynamic diameter particle size ranges. We refer to the sub-10μm and sub-1μm particle size cut ranges using the common convention PM10 and PM1, respectively, where PM is the acronym for *particulate matter*. APP and SGP size-cut switching occurs every 15 min and 30 min, respectively, in order to facilitate ramping of the RH in the

humidograph system that is used to measure the hygroscopic dependence of light scattering (Sheridan et al., 2001). Humidograph data are not reported in this study. Size-cut switching at BND, where there is currently no humidograph system, occurs every six minutes. Aerosol concentrations and optical properties typically demonstrate little change on timescales less than one hour at APP, BND, and SGP so it is assumed that the same aerosols are sampled for both size cuts at these switching rates over a large majority of hours. The EGB system uses a 1 μm cyclone to achieve a fixed D_p < 1 μm particle size cut so PM10 aerosol properties are not available for EGB. Descriptions of the basic inlet design and sampling strategy, including flow rates, tubing sizes and estimated aerosol losses are provided elsewhere (Sheridan et al., 2001; D&O2002).

2.2 Measurements and instruments

This study reports on several primary aerosol measurements, including aerosol light scattering (σ_{sp}), hemispheric backscattering (σ_{bsp}), and absorption (σ_{ap}) coefficients (Table 2). Each of these parameters is measured for both the PM10 and PM1 size ranges (only PM1 for EGB) and used to calculate the radiative effects of sub-1μm particles (PM1). Variability of AOPs measured at the APP, BND, and SGP sites over the 2010-2013 time period is similar for the PM10 and PM1 size cuts so this paper focuses primarily on PM1 AOPs (Sect. 2.5) for consistency with EGB measurements. Annually-averaged PM10 AOPs and their annual cycles are included in the Supplementary Materials that accompany this paper (Table S5 and Fig. S8)

A three-wavelength (3-λ) integrating nephelometer (Model 3563, TSI Inc., St. Paul, MN) is used at all sites for measurement of σ_{sp} (angular range of 7° -170 °) and σ_{bsp} (angular range of 90°-170°). Aerosol light absorption coefficients are determined by filter-based instruments that make measurements at wavelengths close to those of the TSI nephelometer (Table 1). A 3-λ Particle Soot Absorption Photometer (PSAP, Radiance Research, Seattle, WA) is used at APP and SGP for the entire dataset and at BND for a majority of the study period. A single wavelength (1-λ) PSAP is used at EGB. The PSAPs are modified by placing a small (~ 5 W) heater on their internal inlet lines at the connection with the optical block. The temperature of the metal optical block is kept a few degrees higher than the incoming sample air temperature so the RH of the air stream at the

sample and reference filters remains relatively low. The heater is not actively controlled to maintain a specific RH, but RH variability at low RH is not believed to influence the measurements as strongly as RH variability at high RH (Anderson et al., 2003). Laboratory tests indicate that the heater keeps the RH at the filters below 40% most of the time. An RH of 50% at the filter is exceeded only during sampling of very humid air (Sheridan et al., 2012). A new light absorption instrument (Continuous Light Absorption Photometer, CLAP) was recently developed by NOAA/ESRL to eventually replace the PSAP at all stations in the NOAA/ESRL network (Ogren et al., 2013). The CLAP is similar to the PSAP in that particles are collected on a filter of the same material as used in the PSAP and light transmission through the filter is monitored continuously. A major difference between CLAP and PSAP is that instead of a single sample spot, the CLAP has eight sample spots. CLAP filter spots are selected by solenoids that switch to the next sample spot once the filter transmittance drops below a desired limit (typically 0.7). Thus, the CLAP can run eight times as long as the PSAP before requiring a filter change. The similarity in the CLAP and PSAP instrument designs facilitate the same corrections to the measured σ_{ap}. The CLAP replaced the PSAP at BND in March 2012, after a 13-month instrument inter-comparison period. The PSAP/CLAP comparisons made during the overlap period at BND indicate that the CLAP-measured σ_{ap}, when adjusted to common wavelengths, is approximately 2% lower than PSAP-measured σ_{ap} for each of the three measurement wavelengths (Table 1). The CLAP comes with a small heater built into the optics block and is controlled to a set temperature, typically 39 ^{0}C to minimize RH effects during sampling.

2.3 Data processing, quality assurance, and calculated AOPs

Software developed at NOAA is used to log the data at the sites, automatically transmit the data to NOAA, and ingest the data into the NOAA database. The database is accessible to the individual site mentors via virtual machine software. The virtual machine software includes a graphical user interface for reviewing and editing data as well as tools for extracting the data in a variety of formats and for desired averaging times. The data acquisition, processing and virtual machine software, along with documentation, are open-source and freely available from NOAA (http://www.esrl.noaa.gov/gmd/aero/sw.html). Quality-assured data products for each site in the NOAA/ESRL network are uploaded to

the World Data Centre for Aerosols and made available at http://ebas.nilu.no/Default.aspx. The data products available include hourly-averaged aerosol number concentrations (not presented in this paper), σ_{sp}, σ_{bsp}, and σ_{ap} for the PM10 and PM1 size cuts.

Data quality assurance review for each site is typically performed by the site mentor on a weekly basis. Data during periods of instrument or sampling problems and during times of instrument maintenance are invalidated. Absorption data are flagged for periods when the PSAP or CLAP filter transmission drops to less than 0.7 and invalidated when the filter transmission drops below 0.5 because high filter loading increases the σ_{ap} measurement uncertainty (Bond et al., 1999). The lack of PSAP filter changes on weekends at SGP leads to an under-representation of quality-assured Sunday (all day) and Monday (early morning) σ_{ap} hours over the period of this study. Quality-assured σ_{ap} data at SGP are only available for 38% of Sunday thru Monday morning hours during 2010-2013, versus 70-80% of the hours for the rest of the week. Weekend days with low σ_{ap} are thus well- represented at SGP while weekend days with high σ_{ap} (leading to over-loaded PSAP filters) are under-represented. PSAP filters are changed on weekends at the other sites.

Light absorption coefficient measurements at SGP are particularly sensitive to ambient RH fluctuations due to air conditioning cycles, particularly during hot, humid summers. CC2013 did not use SGP σ_{ap} data in their trend analysis for this reason. Excessively high temperatures during the summer months of June-August (and the early part of September) 2010-2012 resulted in high daytime dew points that often were as high as 20 to 22 ºC during the late afternoon. The high sample humidity coincided with unusually high noise in the PSAP. The hours with noisy σ_{ap} data were removed. On average this resulted in a 15% loss or 3.6 hours per day in the data. Since this time, effort was made to lower the sample RH through insulation of the optics block, use of a Nafion drier on the instrument inlet and rerouting the trailer ventilation. Despite the data loss, the SGP summertime σ_{ap} data does not exhibit a remarkable difference compared to the other sites nor does the 2010-2012 time period vary significantly from 2013, when the noise was not as apparent. We include the SGP σ_{ap} data in this paper for the 2010-2013 seasonal, weekly and diurnal cycle studies and the systematic relationships among AOPs. We do not include σ_{ap} or AOPs calculated using σ_{ap} as part of the long term trend analysis.

The four NOAA-ESRL network sites discussed in this paper are located such that there are no major local aerosol sources in the predominant upwind directions, although there are some aerosol sources that are typically downwind but that may occasionally be sampled. Brief spikes in aerosol number concentrations, $\sigma_{sp,}$ σ_{bsp}, and/or σ_{ap} are flagged as local contamination by the site mentor. These spikes are usually 15-20 minutes or less in duration and often coincide with vehicular traffic near the sites or times of peak morning commuter traffic. Broader aerosol peaks are typically retained, as they are characteristic of the sampling environment of the station. One example of a broader aerosol peak not marked as contaminated is elevated σ_{ap} which often persists for hours during mornings with surface inversions or during periods with humid, stagnant air masses.

Hourly averages of σ_{sp}, σ_{bsp}, and σ_{ap} are generated after the data have passed the quality assurance tests. The hourly-averaged σ_{sp} and σ_{bsp} are adjusted to conditions of standard temperature and pressure (T=273.15 K, P=1013.25 hPa) to facilitate σ_{sp} and σ_{bsp} comparisons among the sites. TSI nephelometer measurements are corrected for nephelometer angular non-idealities including truncation effects (Anderson and Ogren, 1998). PSAP- and CLAP-measured σ_{ap} values are corrected for sample area, flow rate, and non-idealities in the manufacturer's calibration as described in Bond et al. (1999) and Ogren (2010). Absorption Ångström exponent values are used to adjust the spectral σ_{ap} values to those at the nephelometer wavelengths so that intensive AOPs involving both instruments (Table 2) can be calculated.

The primary measurements σ_{sp}, σ_{bsp}, and σ_{ap} are used to derive several aerosol properties (Table 2) used in radiative transfer calculations (Haywood and Shine, 1995). These properties have been described in many previous papers (e.g., Sheridan et al., 2001; D&O2002) so only a brief discussion follows. The light extinction coefficient (σ_{ep}) is the sum of the scattering and absorption coefficients. The single-scattering albedo (ω_0) is the fraction of extinction due to scattering, with lower values of ω_0 corresponding to stronger aerosol light absorption. The hemispheric backscatter fraction (b) represents the fraction of light scattered into the backward hemisphere in the nephelometer and provides qualitative information on aerosol size, with larger values of b corresponding to optically active particles with smaller diameters. The scattering and absorption Ångström exponents (α_{sp}

and α_{ap}) describe the wavelength dependence of light scattering and absorption, respectively. The scattering Ångström exponent (typically in the range $0 \leq \alpha_{sp} \leq 3$) provides semi-quantitative information about the aerosol size distribution, with larger values of α_{sp} corresponding to size distributions dominated by smaller particles (van de Hulst, 1957). The absorption Ångström exponent can provide information on aerosol type for certain aerosols (e.g., Cazorla et al., 2013; Bergstrom, et al., 2007). For example, dust and some types of organic carbon (OC) absorb light strongly in the near-UV and blue-violet regions of the electromagnetic spectrum (the so-called "brown carbon"), corresponding to $\alpha_{ap} > 1$ (Cazorla et al., 2013; Costabile et al., 2013). Absorption by black carbon (BC) decreases as λ^{-1} in the near-UV through near-IR, corresponding to $\alpha_{ap} = 1$ (Bergstrom et al., 2002). The sub-1μm scattering and absorption fractions R_{sp} and R_{ap}, respectively, indicate the fractions of PM10 light scattering and absorption due to PM1 particles and serve as a rough proxy for the "fine-mode" fraction of scattering and absorption coefficients.

Haywood and Shine (1995) presented simple equations (Table 2) for calculating top-of-atmosphere (TOA) aerosol DRF and direct radiative forcing efficiency (DRFE) for an optically-thin, partially- absorbing atmosphere. DRFE represents the DRF per unit AOD and is to first-order independent of AOD. If globally-averaged values for all non-aerosol parameters are used (Table 2), the simple equation for DRFE provides a means for comparing the intrinsic forcing efficiency of the aerosols measured at different sites and times, through DRFE dependence on ω_0 and on up-scatter fraction β. The DRFE values themselves are only approximations when globally-averaged values are used. Up-scatter fraction represents the fraction of incoming solar radiation that is scattered by atmospheric aerosols back to space. Up-scatter fraction has been related to b by the approximation of Wiscombe and Grams (1976). A second-order curve fit of the points in their Fig. 3 as reported in Sheridan and Ogren (1999) provides the parameterization shown in Table 2.

2.4 Measurement uncertainties

Detailed measurement uncertainty calculations and discussions are provided in Sect. S1 of the Supplemental Materials and are briefly summarized here. The major sources of uncertainty in σ_{sp} and σ_{bsp} measured by the TSI 3563 nephelometer are (1) instrumental

noise; (2) uncertainty in the nephelometer calibration using filtered air and CO_2 gases; (3) nephelometer calibration variability; (4) uncertainties in the correction for nephelometer angular non-idealities, which result in under-estimation (e.g., truncation) of light scattered in the near-forward direction; (5) uncertainty in correcting σ_{sp} and σ_{bsp} to standard temperature and pressure (STP) conditions; and (6) uncertainties in correcting σ_{sp} and σ_{bsp} to 40% RH during humid conditions. Detailed accounts of uncertainty sources (1)-(5) are given in Anderson and Ogren (1998), Anderson et al. (1999), and Sheridan et al. (2002). The major sources of uncertainty in σ_{ap} measured by the PSAP are (1) instrumental noise; (2) unit-to-unit instrumental variability; and (3) uncertainty in the calibration of PSAP-measured σ_{ap}, using extinction minus scattering as a reference method (Bond et al., 1999). Uncertainties in the PSAP spot size and flow rate corrections are often incorporated into the unit-to-unit variability term (Müller et al., 2011; Anderson et al., 1999). The total measurement uncertainties $\Delta\sigma_{sp}$, $\Delta\sigma_{bsp}$, and $\Delta\sigma_{ap}$ are calculated by adding the major source contributions in quadrature (Anderson and Ogren, 1998). Standard error propagation techniques are applied (Sect. S1 of Supplemental Materials) to calculate uncertainties in intensive AOPs, once $\Delta\sigma_{sp}$, $\Delta\sigma_{bsp}$, and $\Delta\sigma_{ap}$ are estimated and adjustments made for correlations among σ_{sp}, σ_{bsp}, and σ_{ap} (Tables 3, S1-S2). Our reported uncertainties are 95% confidence intervals.

Identical nephelometers, PSAPs, calibration and correction methods are used at the four sites reported in this paper, with the exception of the late replacement of PSAP with the nearly-identical CLAP at BND. As a result, some contributions to the measurement uncertainties are nearly the same for different sites and times and approximately cancel when comparing AOPs between different sites and times, as noted by Anderson et al. (1999). Examples include the nephelometer calibration and STP correction uncertainties. The nephelometer truncation correction uncertainties are also nearly the same, due to the fact that the scattering Ångström exponent used to correct for nephelometer truncation of forward-scattered light (Anderson and Ogren, 1998) exhibits little temporal variability at each of the four sites and is of similar magnitude for each site (Fig. 2g). The PSAP unit-to-unit variability term can be neglected when comparing measurements made at the same site but cannot be neglected when comparing measurements made at different sites. The other uncertainty sources described above must be considered both for intra-site and inter-site

AOP comparisons. We follow a similar methodology to that employed by Anderson et al. (1999). We consider the combined effect of all uncertainty sources which would not be expected to cancel or nearly-cancel when comparing AOPs measured at different sites or times. We refer to their combined effect as measurement precision uncertainty, using the same notation as Anderson et al. (1999). We note that Anderson et al. (1999) did not include the nephelometer RH correction uncertainty nor the PSAP calibration uncertainty in their reported measurement precision uncertainties so our reported measurement precision uncertainties may represent upper bounds. We use the measurement precision uncertainties(Table 3) for comparing AOPs measured at different sites and times. Differences in AOPs between sites/seasons are assessed by comparison with the measurement precision uncertainty ranges (Sect. 2.5). The uncertainties are reported for 1-hour averages but the values differ negligibly for averaging times larger than this (Sect. 1 of Supplemental Materials).

2.5 Data analysis methods

All statistics reported in this paper are based on hourly-averaged, quality-assured σ_{sp}, σ_{bsp}, and σ_{ap} measurements made continuously or near-continuously at APP, BND, EGB, and SGP over the 2010-2013 period. We report only the results for the PM1 size cut at APP, BND, and SGP so as to minimize redundancy and to simplify comparisons with PM1 AOPs measured at EGB. The only exceptions are the use of the more-relevant PM10 scattering Ångström exponent and the sub-1μm scattering and absorption fractions (R_{sp} and R_{ap}), calculated as the ratios of PM1/ PM10 σ_{sp} and σ_{ap}, respectively (Table 2). PM10 AOP variability at APP, BND, and SGP is reported in the Supplemental Materials (Fig. S8 and Table S5). The intensive AOPs (Table 2) are calculated for each hour, using the hourly-averaged σ_{sp}, σ_{bsp}, and σ_{ap} values. For brevity, only AOPs at 550 nm are presented with the exception of the wavelength dependent α_{sp} and α_{ap}. Scattering and absorption Ångström exponents are calculated based on the 450 nm and 700 nm wavelength. We ~~f~~ollow a similar approach to that taken by D&02002 and Andrews et al. (2011) and only use hours for which PM1 σ_{sp} at 550 nm is at least 1.0 Mm^{-1} to calculate the intensive AOP statistics, so as to reduce noise resulting from taking ratios of two small quantities (Table 2). Filtering the intensive AOPs for low-σ_{sp} hours discards 1.4% of the hours at APP, 0.1%

at BND, 1.8% at EGB, and 0.5% at SGP. These percentages are uniform across seasons, except for slightly higher percentages during fall at EGB and SGP (Table S3). We use all hours in calculating σ_{ap}, σ_{sp} and σ_{bsp} statistics, to avoid a bias toward 'less clean' conditions. Lack of PM10 measurements and use of a single-wavelength PSAP preclude calculation of R_{sp}, R_{ap}, and α_{ap} at EGB.

2.5.1 Temporal cycle analysis

Hourly-averaged and quality-assured AOPs are binned by month, day of week, and hour of day to study their annual, weekly, and diurnal cycles, respectively (Sect. 4.1). Geometric means and 95% confidence intervals of the geometric means are calculated for the binned σ_{sp} and σ_{ap}, whose distributions are closer to log-normal than normal. Arithmetic means and 95% confidence intervals of the means are calculated for the binned intensive AOPs, whose distributions are suitably-approximated as normal. Atmospheric variability for each month, day of week, or hour of day is quantified by the 95% confidence intervals of the mean value, which are represented as error bars on the plots. Differences in the mean AOPs are termed 'significant' in this paper if they are larger than ***both*** (1) atmospheric variability (e.g., if the error bars do not overlap); and (2) twice the precision measurement uncertainty (Table 3). We define the magnitude of temporal variability on each of the timescales as the amplitude of the cycle of mean values (difference between maximum and minimum values). Cycle amplitudes are also expressed as percentages by dividing this difference by the midpoint between maximum and minimum values.

Aerosol optical properties at the four sites vary primarily on seasonal timescales. Day of week variability in AOPs can be used as a tool for distinguishing anthropogenic from natural aerosol sources, since natural sources would not be expected to have AOPs that vary on weekly scales (Murphy et al., 2008). Diurnal variability is used along with co-located meteorological data to infer the influence of local pollution sources and mixing layer height on measured AOPs. Due to the dependence of most AOPs on season, their weekly and diurnal cycles are reported for both full years and individual seasons.

2.5.2 Meteorological analysis

Data from co-located surface meteorological stations at the four sites are used to develop

proxies to help explain some features of the AOP cycles at each station. Pollution-rose diagrams showing the dependence of σ_{sp}, σ_{ap}, and some calculated AOPs on wind direction are shown for individual seasons to examine the influences of wind sectors and known regional pollution sources on measured AOPs (Fig(s). 5-8 and S16-S22). We compare the temperature-dependence of σ_{sp} (Fig(s). S5 and S7) with reported temperature dependence of biogenic secondary organic aerosol (SOA) (Leaitch et al., 2011; Goldstein et al., 2009) and ammonium nitrate partitioning (Parworth et al., 2015; Rupakheti et al., 2005). We also use temperature-dependence of σ_{sp} along with monthly-median temperatures at the sites (Fig. S23) and monthly-averaged σ_{sp} (Fig. 2a) to hypothesize the role of photochemistry on the seasonality of σ_{sp}. Mixing layer height climatologies have been reported for locations at or within ~170 km of the sites. We use the seasonal dependence of the reported mixing layer heights to assess the effect of convection (or lack thereof) on the annual and diurnal cycles of measured near-surface σ_{sp} and σ_{ap} at the four sites.

2.5.3 Significance and trend analysis

Mean values of AOPs over the entire 2010-2013 period are calculated for each site and the differences in mean AOPs among the sites are used as a measure of regional variability (Sect. 4.2). Seasonal differences of most AOPs at individual sites are often much larger than the regional differences of annual-mean AOPs so the seasonality of regional AOP differences must also be taken into account. The differences in mean AOPs among the sites are termed ‘significant’ if they satisfy the same two criteria stated in Sect. 2.5.1 for temporal differences. Of the four sites, only BND and SGP have long enough time series (> 10 years) to evaluate trends in AOPs (Sect. 4.3). Slopes and significance are obtained using the function ‘TheilSen’ in the R package ‘openair’ (Carslaw et al., 2012; Carslaw, 2015). Data are de-seasonalized and autocorrelation is accounted for using options supplied with the TheilSen function. Decadal slopes (%/10-year) are calculated by multiplying the yearly slope by 10. Trends are not reported for SGP AOPs requiring absorption due to PSAP data quality issues over most of the 1997-2009 period. Absorption Ångström exponent trends are not calculated for BND because the available time series is less than 10 years.

2.5.4 Systematic relationships

Systematic relationships among intensive AOPs and aerosol loading are explored on an annual basis at the four North American sites for the 2010-2013 (Sect. 4.4). Relationships involving α_{ap} vary with season at some sites so these relationships are also presented for individual seasons. D&O2002 suggested systematic relationships would be useful for constraining model parameterization of AOPs and for reducing uncertainties in satellite-based retrievals of AOD, which make assumptions regarding aerosol size distributions and ω_0 (e.g., Levy et al., 2010). Systematic relationships can also provide information regarding aerosol source types and processes. Relationships between mean intensive AOPs and aerosol loading, represented by σ_{sp} at 550 nm, are investigated for each season at each site by separating hourly-averaged σ_{sp} values into bins of 10 Mm^{-1} width and then calculating the mean AOPs for each σ_{sp} bin. The x-values for the data points on each plot correspond to the bin center. Only bins with a number of data points exceeding 0.1% of all data points are plotted. The relatively high ω_0 values at all sites justifies the use of σ_{sp}, rather than σ_{ep}, as a proxy for loading. Relationships among a few select intensive AOPs are also included to provide more insight into aerosol sources and/or processes influencing the properties measured at the sites.

3 Site descriptions

All four sites in this study are mid-latitude (35-45 ^{0}N) locations in North America with elevations ranging from 230 to 1080 m above sea level (asl), placing them firmly in the boundary layer. These sites can be categorized as anthropogenically-perturbed, rural continental locations. Published aerosol chemistry at the sites (Link et al., 2015; Buzcu-Guven et al., 2007; Rupakheti,et al., 2005; Parworth et al., 2015) indicates that the sites are regionally- influenced.

3.1 Appalachian State University, Boone, North Carolina, USA (APP)

The APP site is situated at the highest point on the Appalachian State University campus (1080 m), located in the southern Appalachian mountain town of Boone, NC (pop. ~20,000). In situ aerosol measurements were initiated at APP in June 2009. APP is also home to a Cimel sunphotometer as part of AERONET, a micro-pulse lidar, an aerosol mass spectrometer, a solar pyranometer as part of the NASA SolRad-Net, and a suite of

meteorological and trace gas measurements. The region surrounding Boone is heavily forested in all directions. The APP site is not located near any major highways or major industry but is located 1- 3 km from local commuter traffic sources during weekday mornings and late afternoons. The APP site is located 40-60 km from the following towns: (1) Lenoir/Hickory (population ~ 60,000) to the SE; and (2) Wilkesboro (population 3,500) to the east. The Charlotte metropolitan area (population 2.5 million) is located approximately 160 km SE of APP and the Piedmont Triangle metropolitan area (population 1.6 million) is located 200-230 km ESE of APP. However, winds are from the SE only ~5% of the time for all seasons (Fig. 5) so the influence of these towns/cities on the APP site is generally small.

Summer AOD in the warm, heavily-forested SE US is influenced by highly temperature-dependent isoprene-derived SOA (Goldstein et al., 2009). The Appalachian mountain region is also home to some of the highest rural ammonium sulfate concentrations in the US, with maximum concentrations in summer and minimum concentrations in fall/winter (Hand et al., 2012b). Link et al. (2015) reported in the Supplement to their paper that non-refractory PM1 aerosol mass at APP during summers (winter) of 2012-2013 was ~66% (49%) organic aerosol, 24% (31%) sulfate, 7% (10%) ammonium, and 3% (10%) nitrate. Approximately 77% of the summer organic aerosol (OA) mass was comprised of low-volatility oxygenated SOA (LV-OOA) and isoprene-derived SOA while the winter OA was comprised of LV- OOA and biomass-burning OA (Link et al., 2015). Wood-burning stoves serve as the primary heating source for 6.2% of occupied housing units in Watauga County (US Census Bureau, 2010) and likely a larger percentage of housing units in the surrounding rural mountain communities. The highly- oxidized, “aged” LV-OOA factor present in nearly equal concentrations during both summer and winter at APP suggests that it is representative of regional background SOA (Link et al., 2015).

Weather patterns affecting the southern Appalachian mountain region are highly diverse due to a variety of factors, including complex topography, mid-latitude location, and proximity to the Gulf of Mexico and Atlantic Ocean. Common weather regimes include winter storms, convective cells, dying tropical cyclones, and stagnant summertime episodes. Wind directions are predominately from the west for all seasons (Fig. 5). Wind speeds are highest in November-March and lowest in May- September. The annual temperature cycle

516 in Boone, NC is relatively small, with average daily high temperatures of ~24-26 ^{0}C in
517 June-Aug and ~5 ^{0}C in January. The annual cycle in average monthly precipitation is also
518 small, with a maximum in summer (12-13 cm) and minimum in October (~9 cm). Relative
519 humidity (RH) is highest during the summer at APP. Planetary boundary layer (PBL)
520 heights calculated from vertical aerosol backscatter profiles measured with a micro-pulse
521 lidar at APP from 2/2013-8/2014 reveal a relatively weak diurnal and seasonal dependence
522 of PBL heights. Median afternoon (morning) PBL heights are 920 m (820 m) in winter, 1200
523 m (880 m) in spring, 1100 m (850 m) in summer, and 1050 m (680 m) in fall (unpublished
524 result).

525 **3.2 Bondville, Ilinois, USA (BND)**

526 The BND aerosol monitoring station is located on farmland at the Bondville
527 Environmental and Atmospheric Research Site (BEARS) in rural east-central Illinois. In situ
528 aerosol measurements at BND began in 1994. Additional measurements made at BND
529 include a Cimel sunphotometer as part of AERONET, a comprehensive set of
530 meteorological measurements, an IMPROVE aerosol chemistry system, and a full suite
531 of solar radiation measurements made by NOAA/ESRL. The BND station is situated
532 approximately 6.5 km south of Bondville (population 450), 16 km southwest of
533 Champaign–Urbana (population ~230,000), and is surrounded in all directions by corn,
534 soybean and hay fields. A regional airport (Willard Airport) is situated approximately
535 10 km east of the BND site. The town of Decatur (population ~75,000) lies ~50 km to
536 the SW and three large metropolitan areas are within 250 km of the site: (1) Chicago
537 (population 9.6 million), located ~240 km to the NNE; (2) Indianapolis, IN (population
538 1.8 million), located ~210 km to the east; and (3) St. Louis, MO (population ~3.7 million) is
539 located ~230 km to the SW. The area is crisscrossed by a network of interstate
540 highways, including I-57 (~7 km to the east), I-72 (~10 km north), I-74 (~15 km
541 northeast), and I-70 (~100 km south).

542 Buzcu-Guven et al. (2007) applied positive matrix factorization techniques to apportion
543 the PM2.5 aerosol mass at BND into the following annually-averaged factors: (1)
544 secondary sulfate (27%); (2) secondary nitrate (24%); (3) mobile/SOA factor (17%), largely
545 due to gasoline and diesel vehicle emissions; (4) biomass-burning OA (12%); (5) soil
546 (6%); (6) copper smelter (2%); (7) chromium and nickel from metal plating (5%); and (8)

mixed industrial (7%). The largest contributors to organic matter (OM) were biomass burning (38% of OM) and mobile/SOA (24% of OM) factors, followed by factors associated with industrial sources (< 20% of OM). Buzcu-Guven et al. (2007) could not resolve the mobile source aerosol factor into the two fuel combustion types (gasoline vehicle and diesel) because the BND site is affected by transported urban emissions rather than local emissions. They reported strong seasonality in secondary sulfate (maxima in summer) and nitrate (maxima in winter) at BND. Similar regional sulfate and nitrate seasonality was reported for the region by Hand et al. (2012b) and by Spak and Holloway (2009). The highest sulfate concentrations at BND were associated with transport from the Ohio River Valley, Western Ohio, and Southern Illinois, where large numbers of coal-fired power plants are located (Buzcu-Guven et al., 2007). Winter ammonium nitrate concentrations in the Midwest US are among the highest in the country, due to significant sources of agricultural ammonia and combustion-generated NO_X emissions, in addition to meteorological conditions (low temperature and high humidity) favorable for gas-to-particle partitioning (Hand et al., 2012b; Spak and Holloway, 2009).

Polluted air at BND is generally associated with southerly wind sectors (120º-240º wind directions) and cleaner air is typically associated with NW wind sectors (Fig. 6). Winds reaching BND from the SW also pass over regions with high summer biogenic isoprene emissions (Fig. 3 of Parworth et al., 2015). Wind speeds are higher in November-May and lower in June-September (not shown). Higher wind speeds are more common for S/SW wind sectors for all seasons except winter, when higher wind speeds are more common for NW wind sectors. Lowest wind speeds are associated with easterly wind sectors. Average high temperatures are highest in July (29.5 ^{o}C) and lowest in January (0.5 ^{o}C). Average monthly precipitation is highest in May-July (~12 cm) and lowest in Jan-Feb (~5 cm). Holzworth (1964) used daily soundings at Joliet, IL (located ~130 km NNE of BND) to calculate monthly mean maximum mixing layer heights: DJF (480, 480, 480 m); MAM (980, 950, 1040 m); JJA (1090, 1380, 1310 m); SON (860, 790, 600 m). Climatologies of surface aerosol optical properties observed at BND have been reported by Koloutsou-Vakakis et al. (2001) and D&O2002. Sheridan et al. (2012) also reported BND surface aerosol properties for comparison with airborne aerosol measurements.

3.3 Egbert, Ontario, Canada (EGB)

The EGB station at the Centre for Atmospheric Research Experiments (CARE), is situated near the town of Egbert, in Ontario, Canada. In situ aerosol optical measurements at EGB began in 2009. The CARE facility is also home to complementary measurements of greenhouse gases such as CO_2 and CH_4, as well as meteorological instrumentation and measurements of aerosol chemistry and aerosol size distributions. Egbert is a rural location consisting of mixed deciduous/coniferous forest and agricultural land. The population of Egbert and surrounding communities is approximately 20,000. Egbert is located 70 km N/NE of Toronto, Ontario and the heavily-populated southern Ontario region, with a population of approximately 8 million. A major highway (HWY 400) is located approximately 8 km to the east of the EGB site. The highway experiences commuter traffic during early morning and late afternoon. The town of Barrie (population ~128,000) is located ~25 km NNE of the EGB site but the wind comes from this direction only ~2-3% of the time for all seasons and the associated air masses are relatively clean (Fig. 7). Forest density is highest to the north of EGB.

Southerly winds (120º-240º wind directions) typically bring more polluted air masses (Fig. 7) associated with outflow from the heavily populated Toronto area, southern Ontario, and eastern US (Yang et al., 2011; Liggio et al., 2010). Southerly air masses contain higher levels of elemental carbon (EC), sulfates, nitrates, and OM and higher EC/OC ratios than cleaner air masses from the north (Chan et al., 2010; Rupakheti et al., 2005; Yang et al., 2011). Organic carbon (OC) and EC are highly-correlated (poorly-correlated) during cold (warm) months, implicating primary aerosol sources during cold months and a large influence of transported warm-season SOA from urban areas south of EGB (Yang et al., 2011). Northerly winds (300º-60º wind directions) typically bring air masses from sparsely-populated, heavily-forested regions (Slowik et al., 2010), with high concentrations of temperature-dependent biogenic SOA during summer months (Leaitch et al., 2011; Slowik et al., 2010). Long-distance transport of smoke from the northwest is also observed during the summer forest fire season in northwest Canada. Wind speeds at EGB are higher in November-April and lowest in July-August. Average daily maximum temperatures are highest in July (26 ºC) and lowest in January (-3 ºC). Holzworth (1964) used daily soundings at Buffalo, NY (located ~170 km SE of EGB) to calculate monthly

mean maximum mixing layer heights: DJF (510, 480, 530 m); MAM (780, 600 810, 1070 m); JJA (1180, 1440, 1360 m); SON (1190, 530, 700 m).

3.4 Lamont, Oklahoma, USA (SGP)

The DOE Southern Great Plains (SGP) Cloud, Aerosol and Radiation Testbed (CART) Central Facility site is located in north central Oklahoma near the town of Lamont (pop. 417) in a rural, agricultural region surrounded mostly by wheat, corn and hay fields. Measurements of in situ aerosol optical properties began in 1996. The site is also equipped with a Cimel sunphotometer (as part of AERONET), cloud radars, lidars, meteorological instruments and many remote-sensing radiometers, making it the largest climate research facility in the world. The SGP site is situated 100-150 km from the following metropolitan areas: (1) Wichita, KS (population ~638,000), located 112 km to the north; (2) Oklahoma City (population 1.3 million), located 136 km to the south; and (3) Tulsa, OK (population ~400,000), located ~150 km to the southeast. The SGP site experiences infrequent local traffic but is situated approximately 15 km to the west of an interstate highway (I-35). There are no major aerosol sources within several hundred km to the northwest, west or southwest of the site.

Parworth et al. (2015) reported an average total non-refractory PM1 aerosol mass concentration at SGP (from November 2010-June 2012) of 7.0 μg m^{-3}. Their reported total aerosol mass concentration was broken down into (1) OA (57%); (2) nitrate (21%); (3) sulfate (12%); (4) ammonium (9.4%); and (5) chloride (0.24%). Organic aerosol constituted a larger and nearly constant mass fraction (~70%) from April-October. Sulfate mass fraction also exhibited little seasonality. Both OA and sulfate mass concentrations demonstrated fall minima, with mass concentrations ~2-3 times lower than during summer. Approximately 90% of the OA was highly-oxidized aged aerosol, with biomass-burning OA comprising the remaining ~10%. The aged, oxidized OA peaked in June-July. Biomass-burning OA was highest in late winter and spring and was likely due to local agricultural burning in preparation for crop season. (Parworth et al., 2015). Ammonium nitrate was the largest PM1 aerosol component in winter, followed by OA. Rural EC concentrations in northern Oklahoma are low and peak in autumn (Fig. 3 of Hand et al., 2013). The super-micron aerosol was primarily soil dust, which exhibits a summer maxima in the region (Hand et al., 2012b).

The typical annual weather cycle at SGP involves a cold, shallow inversion layer in the winter with relatively stagnant winds and a hot, humid summer with strong convection, high daytime boundary layer, and southerly winds. Prevailing winds at the SGP site are from the S/SE for all seasons except winter (Fig. 8). Average high temperatures are highest in July-August (33-34 ^{o}C) and lowest in January (0.7 ^{o}C). Average monthly precipitation is highest in May-June (~11-12 cm) and lowest in Jan-Feb (~3.0-3.5 cm). Median mixing layer heights are less than 100 m (above ground level) from 2030 central standard time (CST) through 0530 CST for all seasons and median afternoon mixing layer heights are 752 m in winter, 1260 m in spring, 1640 m in summer, and 1390 m in fall (DelleMonache et al., 2004). The SW US and southern Great Plains experienced exceptionally hot and dry conditions during 2010-2012, coinciding with La Niña years. Extensive fires raged across the SW US during 2011-2012, particularly Texas, Arizona, Colorado, New Mexico and Oklahoma. The hot, dry conditions during 2010-2012 also created conditions favorable for airborne dust production and transport. Climatologies of surface and aerosol optical properties observed at SGP have been reported by Sheridan et al. (2001) and D&O (2002).

4 Results and Discussion

Several broad features of AOP temporal variability are common to all or most of the four sites. For brevity, these features are first discussed collectively before moving on to a more detailed analysis of AOP variability at each site and then to comparisons among the sites. Much of the seasonal AOP variability at each site can be explained using (1) published results of seasonally-dependent aerosol chemistry at the sites; (2) pollution-rose diagrams, which simultaneously display percentage of hours with winds arriving from each wind sector and the distribution of AOP values for each sector; (3) known regional pollution sources; and (4) published seasonality of PBL height and monthly-median temperature and relative humidity at the sites. Temperature dependence of σ_{sp} is also helpful. Diurnal and weekly cycles of select AOPs and the seasonal dependence of these cycles are used to estimate the relative influences of some local and regional sources (mainly traffic) and PBL heights. Regional variability in AOPs is discussed in the context of the annual AOP cycles and the above-listed sources of seasonal variability at each site. Trends in AOPs at BND and SGP are used to place results for the current period in a long-term context. Systematic relationships among select AOPs at each site are used to help interpret the

temporal and regional AOP variability and to hypothesize aerosol sources or processes at the sites. Numerous pieces of supporting materials for the presented results are included as part of the Supplemental Materials to this paper. We reference those figures and tables with the letter 'S' (ex: Fig. S13, Table S2) to distinguish them from figures appearing in this paper.

4.1 Temporal variability of aerosol optical properties

4.1.1 Temporal variability common to all sites

The annual AOP cycle amplitudes are larger than the weekly and diurnal AOP cycle amplitudes at all sites. Nearly all annual AOP cycles are significant, with cycle amplitudes larger than the 95% confidence intervals of both the monthly-mean AOPs (Fig. 2) and the measurement uncertainties (Table 3). July and/or August σ_{sp} maxima are observed at all sites (Fig. 2a), with steeper σ_{sp} decreases from summer to fall than from summer to spring. Summer-to-spring and summer-to-fall σ_{sp} decreases at EGB and APP are approximately twice the magnitude of those observed at BND and SGP. Scattering coefficient reaches a minima during October at all sites except APP, where it is lowest in December. Absorption coefficient is highest in summer and lowest in winter at all sites (Fig. 2b), although the differences between summer σ_{ap} maxima and the surrounding months are only significant at BND and EGB. Summer-to-autumn σ_{sp} decreases are larger than those of σ_{ap}, leading to minimum ω_0 in October at all sites (Fig. 2e). Hemispheric backscatter fraction is highest in October at all sites (Fig. 2d). The confluence of early-autumn decreases in σ_{sp} and ω_0 and increases in b is indicative of less production and/or more efficient removal of large, highly-scattering particles during early autumn, relative to summer. This effect is most noticeable at EGB and APP (Fig. 2) and also is seen in the summer-spring differences at APP. October ω_0 minima contribute to DRFE maxima (least negative) at EGB and BND but no significant autumn DRFE changes are seen at APP and SGP (Fig. 2f). Photochemistry likely influences the summer σ_{sp} maxima and σ_{sp} that are larger in spring than in fall at all sites. The temperature-dependence of σ_{sp} (Fig. S5) and differences in monthly-median temperatures (Fig. S23) combine to yield predicted differences in σ_{sp} that are of similar magnitude to the large observed summer-spring (July-April) σ_{sp} differences at EGB and APP and to the observed summer-autumn (July-October) σ_{sp} differences at EGB, BND, and

SGP (Fig. 2a). The summer-autumn σ_{sp} difference based on temperature considerations is less at APP than the observed σ_{sp} difference, leading us to hypothesize an additional contributor to the autumn σ_{sp} decrease. Cloud and fog scavenging of large, highly-reflecting particles would be consistent with cooler September temperatures (Fig. 23a), higher RH (Fig. S23b), and cloud cover in September at APP. The inverse relationship between σ_{sp} and b seen in the annual cycles at all sites (Fig(s). 2a and 2d) is indicative of the influence of particle growth (and possibly cloud or fog scavenging) on σ_{sp}. Wet deposition likely impacts σ_{sp} most in summer and least in spring and fall, given the seasonality of precipitation at the sites. Secondary σ_{sp} maxima are observed during winter at all sites except APP (Fig. 2a). When combined with winter σ_{ap} minima, the result is a winter ω_0 maxima at these sites (Fig. 2e).

In contrast to b, the annual R_{sp} and PM10 α_{sp} cycles (Fig(s). 2c and 2g) at APP, BND, and SGP (the sites where these AOPs are calculated) do not demonstrate an obvious relationship with the annual σ_{sp} cycles. Collaud Coen et al. (2007) conducted simulations based on Mie theory to show that b at 550 nm is most sensitive to particle size changes for diameters ~100-300 nm (their Fig. 7 and accompanying discussion). Schuster et al. (2006) combined simulations based on Mie theory with volume size distributions and AOD from AERONET to show that extinction Ångström exponent is relatively insensitive to fine mode effective radius for bi-modal aerosol size distributions and that extinction Ångström exponent may serve as a better indicator of fine-mode aerosol volume fraction than mean particle size. The stronger relationship between the annual b and σ_{sp} cycles (relative to relationships between the cycles of σ_{sp} with either α_{sp} or R_{sp}) suggests that the major seasonal changes in the aerosol size distributions at APP, BND, and SGP may lie at the smaller end of the range of optically-relevant accumulation mode particles (100-300 nm), with shifts toward larger particles in summer and smaller particles in fall. Photochemistry likely plays a role in the observed seasonal cycle of b, especially at APP and EGB. Gas-to-particle conversion onto existing particles is most efficient for the 100-500 nm diameter range, since this is where most of the aerosol surface area typically lies (Seinfeld and Pandis, 1998). Reduced gas to particle conversion in fall (when photochemistry and precursor levels are lower) would impact b more than α_{sp} and R_{sp}.

Absorption Ångström exponent is lowest during summer months and highest during

winter months (Fig. 2h) at APP, BND and SGP (the three sites where α_{ap} can be calculated). The summer-to-winter difference in α_{ap} is clearly larger at APP (~0.9) than at BND and SGP (~0.5). Absorption Ångström exponent values near and below 1 during May-September suggest that black carbon (BC) contributes most to σ_{ap} during these months (Gyawali et al., 2009; Cazorla et al., 2013). Gyawali et al. (2009) performed simulations using Mie theory to show that α_{ap} values much less than 1 are possible (their Fig(s). 8 and 9) when absorbing particles are coated with non-absorbing substances. Clarke et al. (2007) also reported a large number of α_{ap} (470/660 nm) values clustered between 0.7-1.1 for pollution plumes during extensive flights over North America as part the of the INTEX/ICARTT experiment in summer 2004.

Weekly and diurnal cycle amplitudes of σ_{sp} (Fig. 3) and nearly all intensive AOPs observed at the four sites are much smaller than the corresponding annual cycle amplitudes. Weekly and diurnal σ_{ap} cycle amplitudes (Fig. 4) are larger than those of σ_{sp} at all sites and are largest in summer. Weekly σ_{ap} cycles at all sites are marginally significant in fall with σ_{ap} cycle amplitudes approximately twice the σ_{ap} measurement precision uncertainty (Table 3). All sites demonstrate small and/or insignificant weekly σ_{sp} cycle amplitudes (~20% or less) and a lack of weekly σ_{sp} patterns across seasons (Fig. 3). This suggests that weekly σ_{sp} cycles are driven by regional-scale phenomena, where any weekend effects are smoothed out by mixing. The weekly cycles of intensive AOPs are nearly always minimal at all sites (Fig(s). S9-S15).

Similar to the weekly σ_{ap} cycles, the diurnal σ_{ap} cycles are also much larger than diurnal σ_{sp} cycles at all sites. However, the diurnal σ_{ap} variability is only significant during summer and (at all sites except APP) fall. Diurnal cycles of nearly all intensive AOPs are minimal and/or insignificant. Notable exceptions are ω_0 and DRFE during summer and fall. The amplitudes of the diurnal ω_0 cycles are ~0.03-0.04 during summer and fall at all sites (Fig. S12). In most of these cases, ω_0 is lowest during late evening and/or early morning and highest during afternoon. At APP, the ω_0 peak extends from around noon to the early morning hours. Diurnal DRFE cycles (Fig. S13) in turn follow the diurnal ω_0 cycles, due to the lack of diurnal variability in b. Summer and fall DRFE is more negative by ~ 3 W m^{-2} AOD^{-1} during the afternoon than during the surrounding hours (Fig. S13).

The lack of diurnal and weekly variability in mean b, R_{sp}, and α_{sp} indicates that particle size distributions at APP, BND, and SGP likely demonstrate little variability on weekly or daily timescales. D&O2002 reported similar or slightly smaller ω_0 and b diurnal cycle amplitudes for BND and SGP but they did not consider the diurnal cycles for individual seasons.

4.1.2 Temporal variability at APP

Aerosol light scattering and absorption coefficients at APP are dominated by PM1 for all seasons and the relative influence of PM1 varies little with season, as seen by R_{sp} values of 0.80-0.88 (Fig.2c), α_{sp} values of 1.9-2.2 (Fig. 2g), and R_{ap} values of 0.90-0.95 (Fig. S8c). Both σ_{sp} and σ_{ap} are moderately elevated for NE wind sectors, with 0º-90º wind directions (Fig. 5). Median σ_{ap} is ~20-30% higher for NE wind sectors than for the prevalent westerly wind sectors for all seasons except winter, when σ_{ap} for the NE wind sectors is ~2 times higher than σ_{ap} for westerly wind sectors (not shown). Median σ_{sp} is less elevated for the NE wind sectors (typically ~10-15%). Wind sector does not strongly influence median or mean values of most intensive AOPs, although low ω_0 (< 0.80) is more frequently associated with NE wind sectors (Fig. S17a). It should be noted that the prevalent westerly wind sectors represent the confluence of 3-4 (seasonally-dependent) different average air mass back-trajectories, which all typically arrive at APP from the west. Link et al. (2015) reported that aerosol and gas phase chemistry measured at APP displayed a generally homogeneous distribution across source regions. One exception was elevated levels of urban, oil and natural gas, combustion tracers, and OA mass concentrations associated with air mass back-trajectories passing over the polluted Ohio River valley and Appalachian mountain region before arriving at APP with ~0º-90º wind directions (Link et al., 2015).

PM1 σ_{sp} at APP and its seasonality (Fig. 2a) are largely influenced by regional background SOA and sulfate. Biogenic SOA and sulfate both exhibit summer maxima and winter minima in the SE US (Goldstein et al., 2009; Hidy et al., 2014) and both summer and winter non-refractory PM1 aerosol mass at APP are dominated by SOA and sulfate (Supplementary Materials of Link et al., 2015). Summer σ_{sp} at APP is correlated with both OA and sulfate mass concentrations (r=0.60 and r=0.62, respectively). The

791 temperature-dependence of PM1 σ_{sp} at APP during April-October (Fig. S7) also agrees
792 well with the expected temperature dependence of biogenic emissions (Guenther et al.,
793 2006) and with the temperature-dependence of AOD over the SE US (Goldstein et al.,
794 2009). The summer σ_{sp} peak coincides with a distinct minima in b (30-40% lower than all
795 other seasons) and maxima in ω_0 (~0.07 higher than during winter). Aerosol number
796 concentrations measured at APP are also lower in summer than during spring and fall
797 (unpublished result). The confluence of lower concentrations of larger, highly-reflective
798 PM1 particles during months with high regional temperatures, solar irradiance, and RH is
799 consistent with gas-to-particle conversion onto existing particles.

800 The annual σ_{ap} cycle at APP (Fig. 2b) is out of phase with the annual cycle of EC
801 concentrations reported for rural eastern US IMPROVE sites (Hand et al., 2012b). Hand et al.
802 (2012b) cited sources such as residential heating for the fall and winter EC concentration
803 maxima. Absorption coefficient at APP exhibits a summer maximum and a winter
804 minimum, though the summer σ_{ap} maximum is not significantly different from early fall
805 and spring σ_{ap} (to 95% confidence). Absorption Ångström exponents of ~ 1.3-1.4 (Fig.
806 2h) and $\alpha_{sp} > 2$ during colder months (Fig. 2h) suggest a mixture of EC and light-absorbing
807 OC (Fig. 2 of Cazorla et al., 2013). A contribution to σ_{ap} from OC is also consistent
808 with a biomass-burning OA factor in the winter aerosol mass spectra measured at APP
809 (Fig. S2 of Link et al., 2015) and may result from winter residential wood-burning (US
810 Census Bureau, 2010; Zhang et al., 2010). However, the diurnal σ_{ap} cycles (Fig. 4b) suggest
811 an influence from local traffic during all seasons and α_{ap} values of 1 or less for non-winter
812 months suggest that BC is the major contributor to σ_{ap} during these months.

813 APP is the only site to demonstrate consistent weekly σ_{sp} and σ_{ap} cycles across seasons,
814 with the exception of winter. Local commuter traffic likely exerts the largest influence on the
815 diurnal σ_{ap} cycles (Fig. 4b) and possibly the weekly σ_{ap} cycles (Fig. 4a). Diurnal σ_{ap} cycles
816 are only significant at 95% confidence during summer but a similar bi-modal structure is
817 seen for all seasons (Fig. 4b), with morning and late afternoon/early evening commuter
818 peaks. The only sign of weekend local traffic influence is an insignificant Saturday
819 morning peak $\Delta\sigma_{ap}$ ~0.1-0.2 Mm^{-1} present during most seasons (unpublished result),
820 confirming the primary influence of local commuter traffic. The absence of any influence of

diurnal PBL height variation on the diurnal σ_{ap} cycles at APP is consistent with the relatively small afternoon/morning PBL height differences measured at the heavily-forested APP site (unpublished result). PBL height is often poorly defined at APP and may be related to the fact that the APP site is situated on a ridge. The PBL and free troposphere do not fully decouple during the evening. As a result, pronounced late-evening thru early morning σ_{sp} and σ_{ap} maxima that are characteristic of a PBL height influence are not a regular feature of the diurnal cycles at APP (Fig(s). 3b and 4b). Diurnal variability of σ_{sp} and intensive AOPs is insignificant and/or minimal for all seasons (Fig(s). S9-S15), with the exceptions of (1) morning ω_0 decreases (by ~0.02-0.03) DRFE increases (by 2-3 W m^{-2} AOD^{-1}) during all seasons, coinciding with the commuter traffic; and (2) a small summer daytime decrease (0.6 to 0.4) in α_{ap}, possibly due to coating of absorbing particles (Gyawali et al., 2009) or an artifact associated with filter-based σ_{ap} measurements (Lack et al., 2008; Lack et al., 2009).

The spring, summer, and fall weekly σ_{sp} and σ_{ap} cycles at APP (Fig(s). 3a and 4a) are characterized by early week increases leading to broad Wednesday-Friday maxima. Both σ_{sp} and σ_{ap} begin to increase near the time of the Monday morning traffic peak (unpublished result) and decrease over the weekend, coinciding with less weekend traffic. The weekly σ_{sp} and σ_{ap} cycles are likely the result of a build-up of scattering and absorbing aerosols in the PBL during the first half of the week. Sunday σ_{ap} minima and weekly cycle amplitudes of ~25-35% during spring and fall are consistent with the timing and amplitudes of weekly EC concentration cycles reported for the rural US (Murphy et al., 2008) and with weekday-weekend EC concentration differences in the urban US (Bae et al., 2004; Blanchard et al., 2008). Smaller but significant weekly σ_{sp} cycle amplitudes of ~15-20% during spring, summer, and fall are larger than weekly cycles in OC and sulfate reported by Murphy et al. (2008). Absorption coefficient exhibits a larger summer weekly cycle amplitude of ~50% (Fig. 4a) than σ_{sp} (Fig. 3a). Local traffic is less during summer but construction activity and road repairs on the Appalachian State University campus and in town are higher so a larger influence from diesel emissions could be a source for the larger σ_{ap} cycle during summer. Local traffic influences on the weekly and diurnal σ_{ap} cycles during winter may be masked by other sources of EC, such as wood-burning. Small weekly cycles in several intensive AOPs are consistent with the above-discussed local

traffic influence. Single-scattering albedo decreases by ~0.02 from Sun-Wed during fall/winter (Fig. S12) with smaller decreases during spring/summer. DRFE increases by ~2 W m^{-2} AOD^{-1} from Sun-Wed during fall/winter, with smaller insignificant increases in spring/summer (Fig. S13). Absorption Ångström exponent increases during the week by ~0.2 (0.4 to 0.6) during summer, with smaller, insignificant increases (~0.1) during fall and winter (Fig. S15).

4.1.3 Temporal variability at BND

PM1 particles contribute ~76% (72%) to the summer (winter) PM10 σ_{sp} and 88% (~80%) to the summer (winter) PM10 σ_{ap} at BND (Fig(s). 2c and S8c). The annual PM1 and PM10 σ_{ap} and σ_{sp} cycles are similar for all seasons (Fig(s). 2 and S8) so the PM1 AOP cycles at BND are representative of the PM10 aerosol. Many of the same general features of the σ_{sp} annual cycle at BND (Fig. 2a) have been reported by others (D&O2002; Koloutsou-Vakakis et al., 2001), including the July-August σ_{sp} maximum and early-autumn σ_{sp} minimum. D&O2002 reported similar summer-autumn and summer-spring σ_{sp} differences, with median σ_{sp} values in July approximately two times larger than σ_{sp} in October-November and ~1.5 times larger than σ_{sp} in April-May. The σ_{ap} annual cycle reported by D&O2002 was also very similar to that shown in Fig. 2b, except for an October σ_{ap} maxima in their study. Planetary boundary layer heights reported for nearby Joliet, IL by Holzworth (1964) were approximately three times higher in summer than in winter, suggesting that summer aerosol production must be much higher (and/or sinks be much lower) to maintain the observed higher summer aerosol loading in the mixed layer.

Regional aerosol transport associated with southerly wind sectors (SE to SW wind directions) exerts a large influence on σ_{sp} during all seasons (Fig. 6a). Northerly wind sectors (NW to NE wind directions) exert a comparable or larger influence on σ_{sp} during winter months. Much of the light-scattering aerosol arriving from the south is likely secondary sulfate associated with the high-density of coal-burning power plants in southern Illinois and the Ohio River Valley region (Buzcu-Guven et al., 2007). Summer σ_{sp} may also be influenced by biogenic SOA. Median summer temperatures are ~3 ^{o}C higher for SW winds at BND than for SE winds and the forests over SW Illinois and SE Missouri emit high amounts of isoprene during summer (Fig. 3 of Parworth et al., 2015). Scattering

coefficient for SW wind directions exhibits a sharp July peak and the temperature-dependence of σ_{sp} at BND during April-October demonstrates modest agreement (r=0.47, as shown in Fig. S7) with the exponential temperature-dependence of biogenic volatile organic compound emissions (Guenther et al., 2006). The secondary PM1 σ_{sp} peak during winter months at BND (Fig. 2a) may be influenced by temperature dependent gas-to-particle partitioning of regional ammonia and nitric acid into ammonium nitrate. Rupakheti et al (2005) reported that gas-phase ammonia correlated positively with particulate ammonium and nitrate mass concentrations for temperatures below 12 ^{o}C and that more ammonia remained in the gas phase for T > 12 ^{0}C. The temperature dependence of median PM1 σ_{sp} at BND changes sign (positive to negative) for temperatures less than ~10 ^{0}C, nearly doubling as temperature decreases from ~10 ^{0}C to ~ -5 ^{0}C (Fig. S5). The σ_{sp} increase is accompanied by an increase in median ω_0 from 0.89 to 0.96 (Fig. S6); and a decrease in median b from 0.15 to 0.13. Addition of large, highly- scattering PM1 particles at low temperatures is consistent with high winter ammonium nitrate concentrations reported for BND (Buzcu-Guven et al., 2007). Much of the winter σ_{sp} increase is likely due to regional transport from the north. Winter σ_{sp} exhibits the largest increase for northerly wind sectors (Fig. 6a) with winter σ_{sp} a factor of ~1.5-3 larger than spring and fall σ_{sp}. Winter ω_0 and b are highest for the northerly wind directions, with $\omega_0 \geq 0.93$ and b < 0.15 for a majority of the arriving air masses (Fig. S19). Northerly wind sectors are typically associated with colder air mass traveling over regions with high concentrations of ammonium and nitrate precursor gases (Hand et al., 2012b). Temperature-dependent ammonium nitrate production is also consistent with the highly variable timing and magnitude of the winter σ_{sp} peak for individual years (Fig. S2). Lower winter PBL heights during winter (Holzworth, 1964) likely also contribute to elevated winter σ_{sp}. Variability in winter PBL heights could conceivably contribute to winter σ_{sp} variability.

Diurnal σ_{sp} cycles are insignificant for all seasons except for a marginally significant fall amplitude of ~25% (Fig. 3d). Diurnal σ_{ap} cycle amplitudes (Fig. 4d) are much larger than those of σ_{sp} during all seasons except winter. Differences between σ_{ap} and σ_{sp} diurnal cycle amplitudes are largest in summer (~60% versus 10%) and are also non-negligible in fall (~50% versus ~25%) and spring (~40% versus ~20%). Diurnal σ_{ap} and σ_{sp} cycles are both smallest during winter, with cycle amplitudes of ~10%. The influence of diurnal PBL

913 height cycle is clearly seen in the diurnal σ_{ap} cycles (Fig. 4d) and a smaller PBL height
914 influence is seen in the σ_{sp} cycles. The differences between σ_{ap} and σ_{sp} cycle amplitudes
915 during summer and (to a lesser degree) fall and spring suggests a large additional source of
916 scattering aerosols during summer daytime hours. Photochemical aerosol processing is the
917 only source of scattering particles whose diurnal and seasonal dependence can explain
918 the seasonality of differences between the σ_{ap} and σ_{sp} cycle amplitudes. It is also consistent
919 with the seasonality of sulfate mass concentrations reported for BND (Buzcu-Guven et al.,
920 2007). Weekly σ_{sp} cycles are statistically significant for all seasons but the cycle
921 amplitudes are less than 15% for all seasons except fall. Our weekly σ_{sp} cycle amplitude for
922 the entire year (Fig. 3c) is similar to that of Murphy et al. (2008).

923 Regional pollution transport associated with southerly wind sectors also influences the
924 annual σ_{ap} cycle at BND over all seasons (Fig. 6b). Highest σ_{ap} for the southerly wind
925 sectors occurs during summer and fall and southerly winds are most common in summer
926 (Fig. 6a), leading to the summer σ_{ap} maxima (Fig. 2b). Lowest σ_{ap} for the southerly wind
927 sectors occurs during winter and air masses from the less anthropogenically-perturbed
928 W/NW reach the site most frequently in winter (Fig. 6b), leading to the winter σ_{ap} minima.
929 The difference between the month of maximum σ_{ap} (August) and that reported by
930 D&O2002 (October) could be due to differences in the seasonality of wind directions between
931 the two periods. It could also arise due to differences in the seasonality of removal
932 mechanisms such as precipitation between the periods but this would have likely also
933 shifted the month of maximum σ_{sp}.

934 The weekly and diurnal σ_{ap} cycles during summer and autumn (Fig(s). 4c-d) are
935 consistent with a large influence from regional diesel emissions during these seasons and
936 possibly during other seasons, although the weekly and diurnal σ_{ap} cycles are only
937 significant in summer and autumn. Maximum σ_{ap} extends from sunset to sunrise for all
938 seasons (Fig. 4d), with a broad minimum extending from just after sunrise to just before
939 sunset. Large seasonality of PBL heights is obvious in the diurnal σ_{ap} cycles (Fig. 4d),
940 consistent with large (factor of 3) summer-to-winter PBL height differences reported for the
941 region by Holzworth (1964). The absence of early morning and late afternoon local
942 commuter peaks at BND is not surprising, since emissions from interstate highway traffic

and agricultural activity represent the largest local sources of absorbing aerosols. Long-distance trucking comprises a large portion of interstate highway traffic in the region and both this and farming activities typically persist throughout the day. The diurnal σ_{ap} cycles for individual days of the week show the same broad features as the corresponding weekly-integrated diurnal σ_{ap} cycles (Fig. 4d) for all seasons, with the exception of differences between post-dusk and pre-dawn σ_{ap} for individual days of the week (unpublished result). During summer, post-dusk σ_{ap} is slightly larger than pre-dawn σ_{ap} for each day during Monday-Friday, leading to a gradual build-up of absorbing aerosols in the PBL. Post-dusk σ_{ap} is less than pre-dawn σ_{ap} on Saturday and Sunday. The resulting weekly σ_{ap} cycle (Fig. 4c) and the σ_{ap} cycles for individual days suggest a nearly-constant source of absorbing aerosols from sunrise to sunset, with largest emissions from Monday-Friday. Both interstate truck traffic and farming activities are consistent with the observed diurnal and weekly patterns during summer but truck traffic is likely the source more capable of contributing to the large summer diurnal and weekly σ_{ap} cycle amplitudes (60% and 40%, respectively), given the higher summer PBL heights in the region. The fall weekly σ_{ap} cycle (Fig. 4c) also exhibits a build-up of absorbing aerosols from Monday-Tuesday, followed by lower aerosol loading during the remainder of the week. This cycle is not consistent with known weekly cycles in truck traffic or agricultural practices near the site. Scattering coefficient exhibits a similar weekly cycle as σ_{ap} during autumn (Fig. 3c) and the weekly σ_{ap} and σ_{sp} cycle amplitudes are similar (~25%) during fall. Similarities in the autumn weekly σ_{ap} and σ_{sp} cycles could simply be the result of a smaller compensating effect on σ_{sp} from daytime secondary aerosol production during autumn (e.g., less photochemistry) or it could be due to sources of scattering and absorbing aerosols that are more similar in autumn than in summer. Diesel emissions from agricultural activity would seem more capable of contributing to the weekly σ_{ap} cycle during autumn, when PBL heights are lower. Biomass burning is a less likely source, even though Buzcu-Guven et al. (2007) reported a significant biomass-burning influence on OM mass (38%) at BND. Absorption Ångström exponent demonstrates minimal day of week variability during autumn (Fig. S15) and α_{ap} values of 1.1-1.2 are not statistically different from the theoretical value of 1 for BC (Bergstrom, et al., 2012).

4.1.4 Temporal variability at EGB

Annual PM1 σ_{sp} and σ_{ap} cycles at EGB (Fig(s). 2a and 2b) are influenced by more polluted southerly air masses (120º-240º wind directions) during all seasons, along with comparable contributions from less anthropogenically-perturbed W/NW wind sectors during summer months (Fig. 7). Liggio et al. (2010) reported that S/SE wind directions were generally associated with transport from the greater Toronto area and that SW wind directions were often associated with more aged aerosol transported from the Ohio River valley region or other urban areas. Wind speeds are lower in May-October and polluted air masses from the south are typically associated with stagnant air masses ahead of fronts (Yang et al., 2011).

Scattering coefficient is elevated for all wind sectors during summer (Fig. 7a). Warm-season aerosol chemistry at EGB is influenced by temperature-dependent biogenic SOA from forests to the north (Leaitch et al., 2011; Slowik et al., 2010) and by photo-oxidation of anthropogenic pollutants from the south (Chan et al. 2010; Liggio et al., 2010). Scattering coefficients exhibit larger summer increases for the less anthropogenically-perturbed wind sectors (all except 120º-240º wind directions) than for the southerly wind sectors (Fig. 7a). Monthly-median σ_{sp} for the southerly wind sectors are ~1.5 times higher in summer than in spring and autumn, with larger summer σ_{sp} increases (factor of 2-5) for the other wind sectors (unpublished result). The largest summer σ_{sp} increases are for NW wind sectors (Fig. 7a). In addition to biogenic SOA, the NW wind sectors are influenced in summer by regional tourist traffic and by episodic long-range transport of smoke during peak fire season in northwest Canada. However, it is not possible to distinguish the effects of aged smoke from biogenic SOA from forests, based on the available aerosol optical measurements during the 2010-2013 period at EGB. The secondary σ_{sp} peak in winter is influenced by higher σ_{sp} associated with air masses from the S/SW (Fig. 7a), relative to spring and autumn. Winter σ_{sp} for wind directions 150º-240º is ~2 times higher than σ_{sp} from other wind sectors (not shown). Single-scattering albedo is also highest for the 150º-240º wind sectors in winter, with values often 0.95 or above (Fig. S20a). Rupakheti et al. (2007) reported episodic high nitrate concentrations associated with air masses transported from urban areas south of EGB, mostly occurring during cold, humid conditions. Scattering coefficient does not exhibit a noticeable increase with decreasing winter temperatures at EGB

during the 2010-2013 period (Fig. S5). Meteorology likely plays a role in the elevated winter σ_{sp}, as PBL heights in the region are lowest in winter at EGB (Horzworth, 1964).

The annual σ_{ap} cycle (Fig. 2b) is qualitatively similar to annual EC mass concentration cycles reported for EGB (Yang et al. 2011) and for rural IMPROVE sites in the Great Lakes region (Spak and Holloway, 2009). Yang et al. (2011) reported mean EC concentrations (in units of $\mu g\ m^{-3}$) at EGB of 0.83 for summer, 0.71 for fall, 0.49 for winter, and 0.36 for spring. Spak and Holloway reported highest regional EC mass concentrations in summer and lowest in winter, with the June EC maxima ~2.2 times higher than the February EC minima. Our reported summer σ_{ap} maxima in August is 2-2.5 times larger than the broad November-April minima (Fig. 2b).

Urban-influenced influenced SE/S wind sectors are associated with highest σ_{ap} and lowest ω_0 for all seasons (Fig(s). 7b and S20a). Chan et al. (2010) attributed higher σ_{ap}, higher EC concentrations, and lower OC/EC ratios in air masses arriving at EGB from the south to diesel emissions. Absorption coefficients are lowest in winter for all wind sectors and are largest for southerly wind sectors during summer and autumn (Fig. 7b), with monthly-median σ_{ap} ~1.5 times higher in summer/autumn than in spring for these wind sectors. Much larger summer σ_{ap} increases (factors of ~3-7) are seen for westerly and northwesterly wind sectors (wind directions ~240º-360º). Episodic long-distance NW transport during the Canadian wildfire season may contribute to summer σ_{ap} but local/regional tourism traffic is more consistent with the observed summer weekly and diurnal σ_{ap} cycles.

Weekly and diurnal σ_{ap} cycles at EGB are significant in summer, marginally significant in autumn, and insignificant in winter and spring (Fig(s). 4e and 4f). Summer and autumn diurnal σ_{ap} cycle amplitudes are ~50% and summer and autumn weakly σ_{ap} cycle amplitudes are ~40%. The diurnal and weekly cycles in σ_{ap} during summer and autumn at EGB are more complicated than those at the other sites and are likely influenced to varying degrees by several sources, including (1) high volume of regional traffic during summer, largest on weekends; (2) transport of urban-influenced aerosol from the south; (3) diurnal PBL height evolution; and (4) local commuter traffic. Diurnal σ_{ap} cycles for individual days of the week reveal morning commuter peaks from Monday-Friday (unpublished result). Daytime σ_{ap} decreases due to lifting of the PBL height are dampened on each of these days by a large

source of absorbing aerosol. Larger summer increases in σ_{ap} for westerly wind sectors suggests a source in addition to transport from the south. The large additional source is likely regional tourism traffic. Differences between post-dusk and pre-dawn σ_{ap} are small on Monday-Thursday (not shown) but are much larger on Friday (~ 1 Mm^{-1}) and Saturday (~ 2 Mm^{-1}) due to high volumes of weekend traffic. Post-dusk σ_{ap} on Sunday is ~ 3 Mm^{-1} lower than pre-dawn σ_{ap}. The composite effect of these sources is the weekend σ_{ap} maxima and Monday minima during summer (Fig. 4e). The weekend σ_{ap} increase gives rise to a small decrease (0.02 to 0.03) in ω_0 and a small increase (~ 2 W m^{-2} AOD^{-1}) in DRFE (Fig(s). S12-S13) Diurnal σ_{sp} cycles for individual days of the week during summer reveal some of the same features as σ_{ap} (unpublished result) but are further complicated by an additional large source of daytime scattering aerosol, likely photochemical production and transport of SOA.

The autumn diurnal σ_{ap} cycle (Fig. 4e) appears to be more influenced by frequent transport from the south (Fig. 7b), along with less regional traffic than during summer. Monthly-averaged σ_{ap} during September-October (Fig. 2b) remains near summer levels (except for August) but σ_{ap} is much lower for all wind sectors except the urban-influenced southerly wind sectors, for which σ_{ap} was similar in value to summer (Fig. 7b). The diurnal σ_{ap} and σ_{sp} cycles exhibit very little structure during fall so lower fall PBL heights may be partially offset by lower production of scattering and absorbing aerosol and/or more efficient removal mechanisms. Some additional source may be responsible for the early-week increase in σ_{ap}, similar to that observed during autumn at BND (Fig. 4c). The source of absorbing aerosol persists throughout the day and into the evening (not shown) and may be local agricultural activities.

4.1.5 Temporal variability at SGP

PM1 particles contribute ~66% (78%) to the summer (winter) PM10 σ_{sp} and ~85% to both summer and winter PM10 σ_{ap} at SGP (Fig(s). 2c and S8c). The annual PM1 and PM10 σ_{ap} and σ_{sp} cycles are similar (Fig(s). 2a and S8a) so the PM1 AOP cycles at SGP are representative of the PM10 aerosol. The annual PM1 σ_{ap} cycle (Fig. 2b) demonstrates good overall agreement with the annual PM10 σ_{ap} cycle reported by D&O2002 for 1997-

2000, with the exception that their winter σ_{ap} minima extends from November-February while our σ_{ap} minima extends from January-February. The annual PM1 σ_{sp} cycle during 2010-2013 (Fig. 2a) also agrees well with that reported by D&O2002 for most non-winter months. D&O2002 reported a broad summer maxima, with monthly median σ_{sp} values lying ~30-40% above spring and autumn months. Our σ_{sp} cycle during non-winter months differs only by a larger summer-to-autumn σ_{sp} decrease of close to factor of 2. Agreement is worse for winter months. Both D&O2002 and Sheridan et al. (2001) reported minimum σ_{sp} in December and maximum in February, with median February σ_{sp} a factor of ~4 higher than December. Box plots of monthly-binned σ_{sp} for individual 2010-2013 years (Fig. S4) show that median February σ_{sp} at SGP varies by up to a factor of 4 for different years, with somewhat smaller differences between individual January months (factor of ~2) and between individual March months (factor of ~2-3). Much of the inter-annual variability is smoothed out in the monthly-binned σ_{sp} box plot for the entire period (Fig. S3), giving rise to relatively constant monthly-mean σ_{sp} during winter for the current period (Fig. 2a). Lower December σ_{sp} and much higher February σ_{sp} occurred during the period reported by D&O2002 and Sheridan et al. (2001), compared to the period reported here.

Pollution transport from the S/SE impacts PM1 σ_{ap} and σ_{sp} throughout the year (Fig. 8). Wind directions are primarily from the S/SE for non-winter months (especially summer). Air mass back-trajectories show that air masses arriving at SGP from the S/SE often travel over or near large regional populations centers, including Oklahoma City, Tulsa, and (in summer) Dallas/Fort Worth (Parworth et al., 2015). Single-scattering albedo is generally lower for S/SE wind sectors than for the less anthropogenically-influenced westerly and northerly wind sectors, except during summer (Fig. S22a). A large fraction of non-refractory PM1 aerosol mass (~70%) is aged SOA during April-October (Parworth et al., 2015). Many SE trajectories pass over regions of high summer isoprene emissions (Parworth et al., 2015) but the temperature-dependence of σ_{sp} (Fig(s). S5 and S7) is less than for the sites with known biogenic SOA influence (EGB and APP). Absorption Ångström exponent values close to 1 for all seasons (Fig. 2h) suggest that despite high organic composition, light-absorbing OC exerts a minimal influence on the annual σ_{ap} cycle and that most of the absorbing aerosol is BC. Daily averages of α_{ap} can have values that extend to as high as 2.5 (unpublished result), which is consistent with observed plumes of

biomass burning aerosol reported by Parworth et al. (2015). Other than lower σ_{sp} during autumn, σ_{sp} and σ_{ap} for the S/SE wind sectors do not demonstrate much seasonality (Fig. 8). The lack of seasonal variability in mean σ_{ap} and σ_{sp} during non-winter months (relative to the other sites) may be due to a longer distance from the population centers (increased aerosol dispersion) and higher PBL heights at SGP during spring, summer, and autumn. Removal processes may also be more efficient in late spring and summer, when monthly-averaged rainfall at SGP is highest.

The frequency of episodic transport of ammonium nitrate to SGP likely exerts some influence on winter σ_{sp} and its variability. Parworth et al. (2015) reported that ammonium nitrate comprised approximately half of the non-refractory PM1 mass at SGP during the 2010-2011 and 2011-2012 winters and early-springs (e.g., March) (their Fig(s). 2 and 6). Ammonia and NO_x concentrations near SGP are relatively small and high nitrate episodes (mass concentrations > 3 $\mu g\ m^{-3}$) were nearly always associated with temperatures < 3 ^oC and long-distance transport from agricultural states in the Central Great Plains region. Colder temperatures and more frequent long-distance transport passing over these states likely contributed to nearly a factor of 2 higher average ammonium nitrate concentrations during the 2010-2011 winter than the 2011-2012 winter (Parworth et al., 2015). Average OA concentrations were similar between the two winters so variability in ammonium nitrate likely exerted an influence on the ~50% higher average PM1 mass concentration during the 2010-2011 winter. Lower relative humidity during the 2010-2011 winter indicates that less wet deposition could also have contributed to higher PM1 aerosol mass during that winter (Parworth et al., 2015). The frequency of episodically- transported biomass burning aerosol also influences σ_{sp} and σ_{sp} at SGP. Biomass burning aerosol is most prevalent in the spring, when prescribed crop burning in preparation of planting is more common. Parworth et.al. (2015) reported a much larger biomass burning aerosol influence in spring 2011 than spring 2012, primarily in March-April. Differences are observed in the mean σ_{sp} and σ_{ap} between the two springs, in addition to differences in the 50^{th}, 75^{th}, and 95^{th} percentiles between the two springs (Fig. S4). Differences between the two years are more noticeable for σ_{ap} than for σ_{sp}.

Diurnal σ_{ap} cycle amplitudes (Fig. 4h) are near 40% for all seasons except spring

(25%). Only the summer and autumn cycles are statistically significant. Diurnal PBL height effects are clearly visible in the diurnal σ_{ap} cycles (Fig. 4h), as is a lack of commuter influence. Similar to BND, there is no local commuter traffic that would be expected to influence AOP cycles at SGP. No obvious features are seen in the individual day of week σ_{ap} cycles (unpublished result) to indicate a possible role of interstate traffic or agricultural influences in the weekly or diurnal σ_{ap} cycles (Fig(s). 4g-h). This is complicated by biased SGP σ_{ap} observations during the weekends. The diurnal σ_{sp} cycle is insignificant for all seasons (Fig. 3h), which may reflect increased daytime photochemical processing that is somewhat less in the winter months. Larger mid-day decreases in σ_{ap} than σ_{sp} lead to increases in ω_0 of ~0.03. The hemispheric backscatter fraction varies negligibly during the day. The midday increase in ω_0 leads to more negative midday DRFE, by ~3 W m^{-2} AOD^{-1} in all and 2 W m^{-2} AOD^{-1} in summer. The aerosol parameters related to size show contrasting trends. No visible diurnal or weekly trend is apparent in b while α_{sp} shows a decline with larger aerosol in the early evening. The trend in declining afternoon α_{sp} values starts earlier in the day during the winter and is weakest during the summer and spring.

4.2 Regional variability of aerosol optical properties

Regional differences in some annually-averaged AOPs (Fig. 2; Table S5) are unbiased by single months or seasons. PM1 σ_{sp} is highest at BND and lowest at EGB, with annual-mean σ_{sp} 70% higher at BND than at EGB (Fig. 2a). The regional differences in σ_{sp} reflect the fact that the upper Midwestern US is more anthropogenically-influenced than the other three regions, with more large population centers, high concentrations of coal-burning power plants, higher volumes of traffic, and more agricultural activity. Spak and Holloway (2009) concluded that *"PM2.5 is a year-round air quality problem in the upper Midwestern US and Southern Canada, driven by nitrate in the winter, sulfate in the summer, and ammonium, OA, EC, and other components year-round"*. The largest winter σ_{sp} peak at BND may be due to higher levels of regional ammonium nitrate precursors and cold, humid winter conditions favorable for ammonium nitrate production in the upper Midwestern US, where winter ammonium nitrate concentrations are higher than almost all other regions in the US (Hand et al., 2012b). The annual σ_{sp} cycle at APP

(Fig. 2a) is driven almost completely by the seasonality of regional SOA and sulfate production (Goldstein et al., 2009; Hidy et al., 2014) due to the lack of urban influence on AOPs at APP. Both SGP and EGB are located downwind at times from large urban centers but both sites receive only a small anthropogenic contribution from all but southerly wind sectors. More frequent polluted air masses from the south may be the reason for higher σ_{sp} at SGP than at EGB for all but summer months (Fig(s). 7a and 8a).

PM1 aerosol contributes a larger fraction to PM10 σ_{sp} and σ_{ap} at APP than at BND and SGP, as evidenced by higher R_{sp} (Fig. 2c) and higher R_{ap} (Fig. S8c). Both R_{sp} and R_{ap} are the highest at APP for all months. The regional differences in R_{sp} are significant for all months (Fig. 2c). Differences in R_{ap} between APP and BND are only significant for November-March (Fig. S8c). The regional differences in R_{sp} and R_{ap} are likely due to a larger influence of soil dust to PM10 AOPs at SGP and BND. Sea salt concentrations are minimal in all three regions and soil dust concentrations are higher in the agriculturally-influenced Midwestern US and Southern Great Plains than in the Appalachian mountain region (Hand et al., 2012b). Given the higher density of forests near EGB than near BND and SGP, it is likely that R_{sp} and R_{ap} would be higher at EGB (if measured there) than at SGP and BND. A larger regional agricultural influence near EGB than near APP may give rise to R_{sp} and R_{ap} that are slightly lower than those at APP. Other indicators of aerosol size distribution (PM1 b and PM10 α_{sp}) also follow similar seasonal cycles at BND and SGP (Fig(s). 2d and 2g). One notable difference is lower α_{sp} at SGP (by ~ 0.3) for nearly all months. Similar R_{sp} and b values but different α_{sp} could be indicative of differences in the larger part of the accumulation mode (particle diameters close to 1 μm). APP and EGB have very similar b values for warm-season months (May-October), which is likely due to large biogenic SOA influences during the warm season in both regions (Goldstein et al., 2009; Link et al., 2015; Leaitch et al., 2011; Slowik et al., 2010). The highest annually-averaged b at APP amongst the sites (Fig. 2d) is influenced by cold-season months (November-April). EGB is influenced by large, highly-scattering PM1 particles from the south during winter months (Fig. S20). Winter PM1 aerosol at APP is largely regional SOA and sulfate, with some influence from biomass-burning aerosol (Supplemental Materials to Link et al., 2015). Higher b at APP during winter and the surrounding months could be due to less particle growth (photochemistry).

The differences between annually-averaged σ_{ap} among the sites is insignificant (Fig. 2b), based on σ_{ap} precision measurement uncertainties (Table 3). Differences in monthly-mean σ_{ap} among the sites are insignificant for most months. The only exceptions are (1) EGB σ_{ap} is lower than APP in April and lower than APP and BND in November; (2) SGP σ_{ap} is lower than BND in August. The annual σ_{ap} cycle amplitudes are larger at BND and EGB than at APP and SGP. Larger σ_{ap} increases during summer and the surrounding months at BND and EGB are consistent with higher levels of regional traffic during these months. The smaller annual σ_{ap} cycle amplitudes at APP and SGP may be influenced by their further proximity from large urban centers. Biomass-burning aerosols also influence σ_{ap} to some degree at APP during winter (Supplemental Materials to Link et al., 2015) and at SGP during winter and spring (Parworth et al., 2015) and may also dampen the σ_{ap} cycles at APP and SGP. Absorption Ångström exponents (Fig. 2h) support the assertion that biomass burning aerosol may influence winter monthly-mean σ_{ap} at APP in November-February (Cazorla et al., 2013). Monthly-mean α_{ap}, however, is not significantly greater than 1 during any other months at SGP, BND, and APP, given the α_{ap} measurement precision uncertainty (Table 3).

Annually-averaged PM1 ω_0 and DRFE are statistically similar for APP, BND, and SGP. Lower annually-averaged ω_0 (Fig. 2e) and higher (less-negative) annually-averaged DRFE (Fig. 2f) at EGB are marginally-significant (at 95% confidence) and these differences are heavily biased by September and October. The simple use of annually-averaged values to discuss regional ω_0 variability (Fig. 2e) is a bit misleading, given the large seasonal ω_0 variability at BND and EGB (and to a lesser degree-APP and SGP). Monthly-averaged ω_0 at EGB is close to 0.10 lower than that at APP and SGP during September-October and is also 0.08 lower than annually-averaged ω_0 at EGB. Single-scattering albedo differences between APP and BND are nearly this large in winter, despite the fact that annually-averaged ω_0 is statistically indistinguishable at the two sites. The regional ω_0 differences are at least as large as reported ω_0 differences among BND, SGP, and two North American coastal sites - Barrow, Alaska and Sable Island, Nova Scotia (D&O2002). In spite of the high seasonality in ω_0 and b, the co-variation of these two intensive properties lead to insignificant annual DRFE cycles at APP and SGP. Larger DRFE cycle amplitudes are

observed at EGB (~9 W m^{-2} AOD^{-1}) and BND (~6 W m^{-2} AOD^{-1}), with September-October DRFE maxima (least negative (DRFE) at both sites (Fig. 2f).

4.3 Long-term aerosol optical property trends at BND and SGP

Trends in AOPs are calculated for the PM10 and PM1 size cuts at BND and SGP. In general, the sign of the AOP trends are the same for both size cuts, although the magnitudes of the trends differ. With the exception of α_{sp}, where the PM10 value is more meaningful, we focus on the PM1 AOP trends for consistency with the rest of the paper. Statistically significant trends in PM1 σ_{sp} (decreasing), R_{sp} (decreasing), and PM1 b (increasing) are found at BND from 1996-2013 and at SGP from 1997-2013 (Table 4). Visual examination of Figure 9 reveals that the trends in these AOPs since ~2009 are somewhat more pronounced than in earlier years, pointing out the pitfalls associated with trend analysis on short-term time series. Additionally, there is a statistically significant decreasing trend in PM10 α_{sp} at SGP (Table 4; Fig. S24); the BND trend in σ_{ap} is negative but not statistically significant. BND also demonstrates a slight, but statistically significant negative trend in ω_0 (Table 4; Fig. S25). The significant decrease in σ_{sp} at both sites is consistent with other studies (CC2013; Hand et al., 2014) that reported large decreases in near-surface aerosol light scattering and light extinction coefficients in North America during the past decade. The concurrent decreasing trend in R_{sp} implies that scattering by PM1 is decreasing at a faster rate than scattering by super-1μm particles (which may or may not be decreasing) at both BND and SGP. One possible source for reductions in PM1 σ_{sp} at BND and SGP could be decreasing SO_2 emissions by regional power plants. Annual US SO_2 emissions from power plants decreased at a rate of ~6% per year from 2001-2010, with similar reductions in sulfate concentrations at rural US sites (Hand et al., 2012a).

CC2013, performed trend analyses on σ_{sp}, σ_{ap}, α_{sp}, and b at BND and SGP as part of a larger study looking at long term changes in in-situ aerosol properties measured around the globe. There are several key differences between our analysis and that of CC2013 so the magnitudes of the trends should not be directly compared, but the signs of the trends (positive/negative) can be compared. Differences between the two studies include: (1) monthly data are used in our analysis (CC2013 used daily); (2) our trend analysis extends the data sets three more years past that of CC2013; (3) we report trends for both PM10 and PM1

AOPs (CC2013 used PM10 AOPs); and (4) we reference the percent slope to the first year value while CC2013 referenced their slope to the median value of the parameter for the entire data set.

For σ_{sp} and σ_{ap}, the direction (positive/negative) of the trends in CC2013 and this study are the same. CC2013 reported larger trends for σ_{ap} and σ_{sp} than are found here, likely due to a combination of the differences between the two analyses noted above. One noticeable difference between CC2013 and this study is that CC2013 found a statistically significant decrease in BND PM10 σ_{ap} at the $p < 0.05$ level, while the decreasing trend for PM10 σ_{ap} calculated here is not statistically significant. CC2013's analysis also included b and α_{sp} trends at BND and SGP. Unlike the analysis performed here, they found no statistically significant trends in either b or α_{sp} when using the Mann-Kendall test with Sen's slope (MK), although the signs of their MK slopes match what is reported in Table 4 for this study. CC2013 found significant positive trends in b at both sites and a negative trend in α_{sp} at SGP when they applied the generalized least square trend test with autoregressive bootstrap confidence intervals (GLS/ARB). CC2013 hypothesized that this discrepancy could be the result of lower sensitivity of the MK method for trends in normally-distributed data. Most intensive AOPs are closer to normally-distributed than are σ_{sp} and σ_{ap}, a point noted by C2013 and confirmed by the authors using data at the four sites reported in our study. CC2013's trend slope in b using the GLS/ARB method was nearly identical in magnitude (7.7% per 10 year) to our slope for BND (Table 4) while their trend slope in b at SGP was smaller (7.8% per 10 year) than our slope. The trend slope in α_{sp} reported by CC2013 for SGP (- 4.2% at SGP) is very similar to our trend slope (Table 4). CC2013 did not analyze trends in ω_0.

4.4 Systematic relationships among aerosol optical properties

Most systematic relationships amongst AOPs are qualitatively similar for all seasons at each site and are suitably represented by the annual relationships. Several of these annual relationships have also been reported for BND and SGP by others (D&O2002; Andrews et al., 2011) and most are similar to the relationships reported here for BND and SGP. We briefly summarize these relationships (Sect. 4.4.1) and highlight any differences in the BND and SGP relationships for our study period (compared to D&O2002 and Andrews et al., 2011), in addition to any differences in the relationships at BND and SGP and those at APP

and EGB, which have not been studied. Relationships involving α_{ap} are seasonally-dependent (especially at APP) and are hence presented for individual seasons at APP, BND, and SGP in Sect. 4.4.2.

4.4.1 Annual systematic relationships among AOPs

Single scattering albedo increases and b decreases with increasing σ_{sp} at all sites (Fig(s). 10a-b). Hemispheric backscatter fraction demonstrates an inverse relationship with ω_0 over the entire ω_0 range at EGN and for $\omega_0 > 0.85$ at the other sites (Fig. 10c), a condition representative of all months (Fig(s). 2d-e). The co-variability of ω_0 and b leads to a DRFE dependence on σ_{sp} that is statistically insignificant for all sites, with the exception of the lowest σ_{sp} conditions at APP (Fig. 10d). Greater influences by smaller, darker particles under low-loading conditions and by larger, brighter particles under high-loading conditions are seen in the annual σ_{sp}, b, and ω_0 cycles for the four sites in this paper (Fig(s). 2a, 2d, and 2e) and have been reported for SGP and BND by D&O2002. The tendency toward lower ωo and higher b for low-loading conditions is consistent with preferential removal of large, less-absorbing particles by cloud scavenging and/or wet deposition. It can also be the result of new particle formation with growth by condensation and/or coagulation to optically-active sizes (Andrews et al., 2011). Scattering Ångström exponent and R_{sp} are both relatively insensitive to changes in σ_{sp} at APP over the entire σ_{sp} range (Fig(s). 10e-f). Scattering Ångström exponent is insensitive to changes in σ_{sp} for all but the lowest aerosol loading levels at BND and SGP (Fig. 10e). PM1 scattering fraction shows a modest decrease with increasing σ_{sp} for σ_{sp} >20 Mm^{-1} at BND and SGP (Fig. 10f). A similar lack of sensitivity of α_{sp} to changes in σ_{sp} at SGP and BND was reported by D&O2002. PM1 scattering fraction increases proportionally with α_{sp} at APP, BND, and SGP (Fig. 10g). D&O2002 reported similar R_{sp} vs. α_{sp} relationships for SGP and BND. The fact that the R_{sp} vs α_{sp} relationship is much stronger than either of their relationships with σ_{sp} suggests that α_{sp} is a better indicator of the relative contributions of coarse and fine mode aerosol to PM10 σ_{sp} than an indicator of average particle size-at least for APP, BND, and SGP. Based on the range of R_{sp} values measured at SGP, BND, and APP (Fig. 2c), the aerosol size distributions are on average bi-modal (with higher coarse mode fractions at SGP and BND than at APP) and care must be exercised when using α_{sp} to infer average particle size or aerosol type. The

R_{sp} vs α_{sp} relationship (Fig. 10g) is consistent with decreasing trends in both R_{sp} and α_{sp} at SGP (Table 4) but seems inconsistent with the lack of change in α_{sp} at BND, despite reductions in R_{sp} similar in magnitude to those at SGP.

AOPs at the rural continental sites reported here have similar relationships (Fig. 10) as those at a majority of mountain sites reported on by Andrews et al. (2011). Andrews et al. (2011) also reported relationships amongst AOPs based on long-term aircraft measurements made over BND and SGP, although their free tropospheric AOP relationships for BND and SGP only extended up to σ_{sp} ~ 25 Mm^{-1}. Most of the free troposphere AOP relationships reported for SGP (Andrews et al., 2011) are similar to the corresponding near-surface AOP relationships (Fig. 10) but there are some noticeable differences for BND. Andrews et al. (2011) reported the following AOP relationships as σ_{sp} increased from zero to 25 Mm^{-1} at BND: (1) b increased slightly (0.12 to 0.13); (2) ω_o remained nearly constant (less than 0.01 increase); and (3) α_{sp} increased by a larger amount (~0.12 to 0.17) than in our study (Fig. 10e). The differences between these relationships and those in Figures 10a, 10b, and 10e could be due to smaller particles that undergo less atmospheric processing (particle growth, cloud scavenging, and deposition) in the free troposphere above BND, relative to particles near the surface.

4.4.2 Seasonal relationships involving absorption Ångström exponent

The relationships between α_{ap} and σ_{sp} for individual seasons and the annual relationship are most different at APP (Fig. 11a) and least different at BND (Fig. 11b). Absorption Ångström exponent at APP is statistically higher than 1 ($\alpha_{ap} \geq 1.2$) for all σ_{sp} bins during winter and is statistically lower than 1 ($\alpha_{ap} \leq 0.8$) for all σ_{sp} bins during summer and for higher-loading conditions ($\sigma_{sp} \geq 50$ Mm^{-1}) during spring and autumn (Fig. 11a). Absorption Ångström exponent at BND (Fig. 11b) and SGP (Fig. 10c) is not statistically different from 1 for any σ_{sp} bins except for (1) summer loading $\sigma_{sp} \geq 30$ Mm^{-1}; and (2) spring and autumn loading $\sigma_{sp} \geq 80$ Mm^{-1} (SGP only). Relationships among α_{ap} and intensive AOPs (α_{sp} and ω_0) can be used to identify contributions to σ_{ap} by sources other than BC, such as dust, OC, and coated BC (Cazorla, et al., 2013; Costabile et al., 2013; Gyawali et al., 2009). Absorption Ångström exponent exhibits a systematic decrease with increasing α_{sp} for all seasons at SGP (Fig. 11f) and α_{sp} decreases in a step-wise manner for all seasons except

summer at BND (Fig. 11f). The α_{ap} - α_{sp} relationship is more complicated at APP, (Fig. 11d), where α_{ap} demonstrates a similar decrease with increasing α_{sp} during summer to that observed at BND but a marginally-significant increase with increasing α_{sp} during winter. Values of α_{ap} that are statistically higher than 1 ($\alpha_{sp} \geq 1.2$) tend to be associated with $\alpha_{sp} \geq 1.5$ at APP (Fig. 11d), suggesting a mix of EC and OC (Fig. 2 of Cazorla, et al., 2013). Values of $\alpha_{sp} \geq 1.2$ at BND and SGP are most often associated with $\alpha_{sp} < 1$ (Fig(s). 11e-f), suggesting a mix of EC and dust (Fig. 2 of Cazorla et al., 2013). Dust influences σ_{ap} at SGP during all seasons and also influences BND σ_{ap} during autumn, as seen by the number of data points with $\alpha_{sp} \geq 1.2$ and $\alpha_{sp} < 1$ in Fig(s). 11e-f. Episodic biomass burning that impacts SGP during spring (Parworth et al., 2015) also contributes to high α_{ap} values, which can reach ~2.5 for individual days (unpublished result). Summer values of α_{ap} are lower than those of other seasons for all α_{sp} bins at BND and APP and for all but the lowest α_{sp} bins at SGP (where dust likely influenced absorption). The slopes of the α_{ap} vs α_{sp} curves indicates that α_{ap} values significantly lower than 1 during summer coincide with higher fractions of fine-mode aerosol (higher α_{sp}).

The annual α_{ap}-ω_0 relationships for all individual seasons are also most similar at BND (Fig. 11h) and least similar at APP (Fig. 11g), where the summer and winter α_{ap}-ω_0 relationships are noticeably different. Absorption Ångström exponent is lowest over the entire ω_0 range during summer at all sites. All of the individual season α_{ap}-ω_0 curves are similar in that α_{ap} remains constant or slightly increasing with increasing ω_0 until ω_0 approaches 0.90 (specifically the ω_0 bin centered at 0.875). This is followed by sharp decreases in α_{ap} with further increases in ω_0. Absorption Ångström exponents significantly less than 1 ($\alpha_{ap} \leq 0.8$) during summer months coincide with $\omega_0 \geq 0.85$ at APP, $\omega_0 \geq 0.90$ at BND, and $\omega_0 \geq 0.95$ at SGP. Absorption Ångström exponent at APP is also significantly less than 1 for $\omega_0 \geq 0.95$ during autumn. From the b vs. ω_0 relationships (Fig. 10c), the lower mean α_{ap} values at all sites during summer also coincide with lower mean b values. When combined, these relationships indicate that lower α_{ap} values are associated with larger, less-absorbing, fine-mode particles. Gyawali et al. (2009) reported a similar α_{ap}-ω_0 relationship for summer months with no biomass burning influence in Reno, NV. Single-scattering albedo was near constant (α_{ap} ~1.1-1.2) up to ω_0 ~ 0.90, followed by α_{ap} values

mostly below one for higher ω_0. Gyawali et al. (2009) attributed this wavelength dependence of absorption to EC particles coated with non-absorbing organic and inorganic matter. It should be noted that Gyawali et al. (2009) used a photo-acoustic spectrometer, as compared to the filter-based techniques that are employed at the sites in this study. Gyawali et al. (2009) also used different wavelengths (405 nm and 870 nm) so the results are not directly comparable. The summer values of α_{ap} at APP are also much lower for all ω_0 than those reported by Gyawali et al. (2009). Possible biases in filter-based absorption measurements made in high-OA environments could in principle contribute to this result (e.g., Lack et al., 2008; Lack et al., 2009). A detailed analysis of the effects, both real and artifact, of absorbing and non-absorbing coatings on the wavelength-dependence of light absorption by black carbon is beyond the scope of this paper.

5 Summary and conclusions

Seasonal variability of nearly all PM1 AOPs is generally much larger than weekly and diurnal AOP variability at the APP, BND, EGB, and SGP surface aerosol monitoring stations. All sites exhibit summer σ_{sp} maxima (Fig. 2a) and broader summer σ_{ap} maxima (Fig. 2b). Secondary winter peaks in σ_{sp} are observed at all sites except APP and coincide with minimum σ_{ap}. Scattering coefficient is lowest at all sites except APP during autumn. Low autumn σ_{sp} coincides with ω_0 minima (Fig. 2e) and b maxima (Fig. 2d) at all sites. In spite of the high seasonality in ω_0 and b, the co-variation of these two intensive properties lead to insignificant annual DRFE cycles at APP and SGP. Larger DRFE cycle amplitudes are observed at EGB (~40%) and BND (~25%), with September-October DRFE maxima (least negative (DRFE) at both sites (Fig. 2f). Regional differences in annual mean AOPs are in general much less than their seasonal variability at individual sites (Fig. 2), requiring that studies of regional AOP variability be conducted on a seasonal basis. Amplitudes of diurnal and weekly cycles in σ_{ap} at the sites (Fig. 4) are larger for all seasons than those of σ_{sp} (Fig. 3), with the largest differences occurring in summer. The weekly and diurnal cycle amplitudes of most intensive AOPs are minimal in most cases, especially those related to parameterizations of aerosol size distribution. Statistically- significant trends in σ_{sp} (decreasing), R_{sp} (decreasing), and b (increasing) are found at BND from 1996-2013 and at SGP from 1997-2013 (Table 4). A statistically significant decreasing trend in α_{sp} is also observed for SGP but not BND.

Systematic relationships among ω_0, σ_{sp} and b (Fig(s). 10a-d) show that high aerosol loading conditions are associated with larger, less absorbing particles and that low aerosol loading conditions are associated with smaller, more absorbing particles for all sites and seasons. These relationships are consistent with other studies (D&02002; Andrews et al., 2011) and suggest the influences of particle growth, wet deposition, and cloud/fog scavenging of larger, less-absorbing particles on σ_{sp} and b (Andrews et al., 2011). Systematic relationships among α_{ap}, σ_{sp}, and α_{sp} (Fig(s). 11a-f) suggest that aerosol light absorption is largely due to EC for all sites and seasons, with the exception of a mixture of EC and light-absorbing OC during winter at APP. Dust and OC likely influence σ_{ap} episodically at SGP (Fig(s). 11c and 11f). The α_{ap}-α_{sp} relationships for SGP (Fig. 11f) and BND (Fig. 11e) are consistent with a mixture of EC and dust for the majority of higher α_{ap} values ($\alpha_{sp} \geq 1.2$) at SGP during all seasons and BND during autumn. The relationships between α_{ap} and ω_0 indicate that values of α_{ap} significantly less than 1 are associated with weakly-absorbing particles. When combined with the ω_0-b relationships (Fig. 10c), the confluence of low α_{ap}, high ω_0, and low b may suggest an influence of coated EC on low σ_{ap} during summer (Gyawali et al., 2009). More detailed studies involving aerosol chemistry and size distributions are clearly needed to state this more definitively.

Many general features of the annual σ_{sp} and σ_{ap} cycles and the weekly and diurnal σ_{ap} cycles at the sites are explained (Sect(s) 4.1.1-4.1.5) in a self-consistent manner using (1) pollution-rose diagrams showing the seasonality of pollution transport (Figs. 5-8); (2) published aerosol chemistry at the sites (Link et al., 2015; Parworth et al., 2015; Yang et al., 2011 and references therein; Buzcu-Guven et al., 2007); (3) temperature-dependence of some known regional σ_{sp} sources; and (4) reported seasonality of PBL heights for the regions. One exception deals with the σ_{ap} cycles at APP. The influence of local traffic is seen in the diurnal σ_{ap} cycles (Fig. 4b) and possibly the weekly σ_{ap} cycles (Fig. 4a). Local and regional wood-burning influence during winter is also consistent with reported aerosol chemistry at APP (Supplemental Materials to Link et al., 2015) and with winter-month α_{ap} values (Fig. 2h) and their relationship with α_{sp} (Fig. 11d). However, neither of these sources nor the seasonality of transport of moderately-elevated σ_{ap} from the northeast (Fig. 5b) adequately explain the annual σ_{ap} cycle at APP. More studies are also needed to better understand

the differences in σ_{ap} and σ_{sp} cycle amplitudes on weekly and diurnal timescales, especially in summer. The potential influence of photochemistry on the annual σ_{sp} cycles is consistent with published aerosol chemistry at the sites. We hypothesize that local photochemical aerosol production could also provide the large daytime source of scattering aerosols during summer and surrounding months that counteracts diurnal PBL height variation, leading to much smaller diurnal cycles in σ_{sp} than σ_{ap}. However, the available datasets in this study are not sufficient to test this hypothesis. Relationships between AOPs and meteorology are also necessary to better understand the effects of atmospheric processing on AOPs at the four sites and their annual and diurnal cycles.

Acknowledgements

Funding for obtaining and evaluating the data came from the DOE ARM program, NOAA Climate Program Office, Appalachian State University College of Arts and Sciences, and Environment Canada, Atmospheric Science and Technology Directorate. We thank the technicians, students, and support staff at all the sites for the dedication and diligence, 24/7/365, required to produce the data sets reported here.

References

Anderson, T.L. and Ogren, J. A.: Determining aerosol radiative properties using the TSI 3563 1400 integrating nephelometer, Aerosol Sci. Technol., 29, 57-69, 1998.

Anderson, T.L., Covert, D.S., Wheeler, J.D., Harris, J. M., Perry, K.D., Trost, B.E., Jaffe, D.J., and Ogren, J.A.: Aerosol backscatter fraction and single-scattering albedo: Measured values and uncertainties at a coastal station in the Pacific Northwest, J. Geophys. Res., 104, D21, 26793-26807, doi:10.1029/1999JD900172, 1999.

Anderson, T.L., Masonis, S.J. Covert, D.S., Ahlquist, N.C., Howell, S.G., Clarke, A.D., and McNaughton, C.S . : Variability of aerosol optical properties derived from in situ aircraft measurements during ACE-Asia, J. Geophys. Res., 108, D23, 8647, doi:10.1029/2002JD003247,.2003.

Andreae, M.O., Jones, C.D., and Cox, P.M.: Strong present-day aerosol cooling implies a hot future, Nature, 435, 1187-1190, 2005.

Andrews, E., Sheridan, P.J., Ogren, J.A., and Ferrare, R.: In situ aerosol profiles over the

Southern Great Plains cloud and radiation test bed site: 1. Aerosol optical properties, J. Geophys. Res. 109, D06208, doi:10.1029/2003JD004025, 2004.

Andrews, E., Ogren, J.A., Bonasoni, P., Marinoni, A., Cuevas, E., Rodriguez, S., Sun, J.Y., Jaffe, D.A., Fischer, E.V., Baltensperger, U., Weingartner, E., Collaud Coen, M., Sharma, S., Macdonald, A.M., Leaitch, W.R., Lin, N.-H., Laj, P., Arsov, T., Kalapov, I., Jefferson, A., and Sheridan, P.: Climatology of aerosol radiative properties in the free troposphere, Atmos. Res., 102, 365-393, 2011.

Bae M., Schaur, J.J., DeMinter J.T., and Turner, J.R.: Hourly and daily patterns of particulate- phase organic and elemental carbon concentrations in the urban atmosphere, J. Air & Waste Manage. Assoc, 54:7, 823-833, DOI: 10.1080/10473289.2004.10470957, 2004.

Bergstrom, R. W., Russell, P. B., and Hignett, P. B.: The Wavelength Dependence of Black Carbon Particles: Predictions and Results from the TARFOX experiment and Implications forthe Aerosol Single Scattering Albedo, J. Atmos. Sci., 59, 567–577, 2002.

Bergstrom R.W., Pilewskie P., Russell, P. B., Redemann, J.,, Bond, T. C., Quinn, P. K., and Sie, B.: Spectral absorption properties of atmospheric aerosols, Atmos. Chem. Phys., 7, 5937–5943, 2007.

Blanchard, C.L., Tanenbaum, S., and Lawson, D.R.: Differences between weekday and weekend air pollution levels in Atlanta,; Baltimore; Chicago; Dallas-Fort Worth; Denver; Houston; New York; Phoenix; Washington,DC; and surrounding areas, J. Air & Waste Manage. Assoc. 58, 1598–1615, DOI:10.3155/1047-3289.58.12.1598, 2008.

Bond, T. C., Anderson, T. L., and Campbell, D.: Calibration and inter-comparison of filter-based measurements of visible light absorption by aerosols, Aerosol Sci. Technol., 30, 582-600, doi 10.1080/027868299304435, 1999.

Buzcu-Guven, B., Brown, S.G., Frankel, A., Hafner, H.J., and Roberts P.T.: Analysis and apportionment of organic carbon and fine particulate matter sources at multiple sites in the midwestern United States, J. Air Waste Manage. Assoc., 57, 606– 619, 2007.

Carslaw, D.C. “The openair manual — open-source tools for analysing air pollution data,” Manual version 1.1-4, King’s College London, 2015.

Carslaw, D.C. and K. Ropkins, “openair — an R package for air quality data analysis,”

Environmental Modelling & Software, vol 27-28, pp. 52–61, 2012.

Cazorla, A., Bahadur, R., Suski, K.J., Cahill, J.F., Chand, D., Schmid, B., Ramanathan, V., and Prather, K.A.: Relating aerosol absorption due to soot, organic carbon, and dust to emission sources determined from in-situ chemical measurements, Atmos. Chem. Phys., 13, 9337–9350, doi:10.5194/acp-13-9337-2013, 2013.

Chan, T. W., Huang, L., Leaitch, W. R., Sharma, S., Brook, J. R., Slowik, J. G., Abbatt, J. P., Brickell, P. C., Liggio, J., Li, S.-M., and Moosmüller, H.: Observations of OM/OC and specific attenuation coefficients (SAC) in ambient fine PM at a rural site in central Ontario, Canada, Atmos. Chem. Phys., 10, 2393-2411, doi:10.5194/acp-10-2393-2010, 2010.

Clarke, A., McNaughton C., Kapustin,V., Shinozuka,V., Howell, S., Dibb, J., Zhou, J., Anderson, B., Brekhovskikh, V., Turner, H., and Pinkerton, M.: Biomass burning and pollution aerosol over North America: Organic components and their influence on spectral optical properties and humidification response, J. Geophys Res., 112, D12S18, doi:10.1029/2006JD007777, 2007.

Collaud Coen, M., Weingartner, E., Nyeki, S., Cozic, J., Henning, S., Verheggen, B., Gehrig, R., and Baltensperger, U.: Long-term trend analysis of aerosol variables at the high-alpine site Jungfraujoch, J. Geophys. Res., 112, D13213, doi:10.1029/2006JD007995, 2007.

Collaud Coen M.,, Andrews, E., Asmi, A., Baltensperger, U., Bukowiecki, N., Day, D., Fiebig, M., Fjaeraa, A.M., Flentje, H., Hyv¨arinen, A., Jefferson, A., Jennings, S.G., Kouvarakis, G., Lihavainen, H., Lund Myhre, C., Malm, W.C., Mihapopoulos, N., Molenar, J.V., O'Dowd, C., Ogren, J.A., Schichtel, B.A., Sheridan, P., Virkkula, A., Weingartner, E., Weller, R., and Laj, P.: Aerosol decadal trends – Part 1: In-situ optical measurements at GAW and IMPROVE stations, Atmos. Chem. Phys., 13, 869–894, doi:10.5194/acp-13-869-2013, 2013.

Costabile, F., Barnaba, F., Angelini, F., and G. P. Gobbi, G.P.: Identification of key aerosol populations through their size and composition resolved spectral scattering and absorption, Atmos. Chem. Phys., 13, 2455-2470, doi:10.5194/acp-13-2455-2013, 2013.

Delene, D. J., and Ogren, J. A.: Variability of aerosol optical properties at four North American surface monitoring sites, J. Atmos. Sci., 59, 1135-1150, 2002.

Dubovik, O., Smirnov, A., Holben, B. N., King, M. D., Kaufman, Y. J., Eck, T. F., and

1513 Slutsker, I.: Accuracy assessments of aerosol optical properties retrieved from Aerosol
1514 Robotic Network (AERONET) Sun and sky radiance measurements, J. Geophys. Res., 105,
1515 9791–9806, 2000.

1516 Dubovik, O., Holben, B., Eck, T.F., Smirnov, A., Kaufman, Y.J., King, M.D., Tanre, D., and
1517 Slutsker, I.: Variability of absorption and optical properties of key aerosol types
1518 observed in worldwide locations, J. Atmos. Sci., 59, 590-607, 2005

1519 Goldstein, A.H., Koven, C.D., Heald, C.L., and Fung, I.Y.: Biogenic carbon and
1520 anthropogenic pollutants combine to form a cooling haze over the southeastern United
1521 States. P. Natl. Acad. Sci. USA, 106, 8835-8840, doi:10.1073/pnas.0904128106, 2009.

1522 Guenther, A., Karl, T., Harley, P., Wiedinmyer, C., Palmer, P.I., and Geron, C.: Estimates
1523 of global terrestrial isoprene emissions using MEGAN (Model of Emissions of Gases and
1524 Aerosols from Nature), Atmos. Chem. Phys., 6, 3181–3210, 2006.

1525 Gyawali, M., Arnott, W. P., Lewis, K., and Moosmuller, H.: In situ aerosol optics in Reno,
1526 NV, USA during and after the summer 2008 California wildfires and the influence of
1527 absorbing and non- absorbing organic coatings on spectral light absorption, Atmos. Chem.
1528 Phys, 9, 8007–8015, 2009.

1529 Hand, J.L., Schichtel, B. A., Malm, W. C., and Pitchford, M. L.: Particulate sulfate ion
1530 concentration and SO2 emission trends in the United States from the early 1990s through 2010,
1531 Atmos. Chem. Phys., 12, 10353–10365, doi:10.5194/acp-12-10353-2012, 2012a.

1532 Hand, J.L., Schichtel, B.A., Pitchford, M. L., Malm, W. C., and Frank, N.H.: Seasonal
1533 composition of remote and urban fine particulate matter in the United States, J. Geophys.
1534 Res., 117, D05209, doi:10.1029/2011JD017122, 2012b.

1535 Hand, J.L., Schichtel, B.A., Pitchford, M. L., Malm, W. C., and Frank, N.H.: Spatial and
1536 temporal trends in $PM_{2.5}$ organic and elemental carbon across the United States, Advances
1537 in Meteorology, 2003, 367674, http://dx.doi.org/10.1155/2013/367674, 2013.

1538 Hand, J.L, Schichtel, B.A., Malm, W.C., Copeland, S., Molenar, J.V., Frank, N., and
1539 Pitchford, M.: Widespread reductions in haze across the United States from the early
1540 1990s through 2011, Atmos. Environ., 94, 671-679, doi: 10.1016/j.atmosenv.2014.05.062,
1541 2014.

\Haywood, J. M., and Shine, K. P.: The effect of anthropogenic sulfate and soot aerosol on the clear sky planetary radiation budget, Geophys. Res. Lett., 22, 5, 603-606, doi:10.1029/95GL00075, 1995.

Hidy, G.M., Blanchard, C.L., Baumann, K., Edgerton, E., Tanenbaum, S., Shaw, S., Knipping, E., Tombach, I., Jansen, J., and J. Walters.: Chemical climatology of the southeastern United States, 1999-2013, Atmos. Chem. Phys., 14, 11893-11914, 2014.

Holzworth, G.C..: Estimates of mean maximum mixing depths in the contiguous United States, Mon. Weather. Rev., 92 235-242, 1964.

Kahn, R. A., Yu, H., Schwartz, S.E., Chin, M., Feingold, G., Remer, L.A., Rind, D., Halthore, R., and DeCola, P.: Introduction, in Atmospheric Aerosol Properties and Climate Impacts, A Report by the US Climate Change Science Program and the Subcommittee on Global Change Research. [Mian Chin, Ralph A. Kahn, and Stephen E. Schwartz (eds.)], National Aeronautics and Space Administration, Washington, D.C., USA, 2009.

Koloutsou-Vakakis, S., Carrico, C.M., Kus, P., Rood, M.J., Li, Z., Shrestha, R., Ogren, J.A., Chow, J.C., and Watson, J.G.: Aerosol properties at a midlatitude Northern Hemisphere continental site, J. Geophys. Res., 106, D3, 3019-3032, doi:10.1029/2000JD900126, 2001.

Lack,D.A., Cappa, C.D., Covert, D.S., Baynard, T., Massoli, P., Sierau, B., Bates, T.S., Quinn, P.K., Lovejoy, E.R., and Ravishankara, A. R.: Bias in Filter-Based Aerosol Light Absorption Measurements Due to Organic Aerosol Loading: Evidence from Ambient Measurements, Aerosol Sci. Technol, 42, 1033–1041, doi: 10.1080/02786820802389277, 2008.

Lack, D.A., Cappa, C.D., Cross, E.S., Massoli, P., Ahern, A.T., Davidovits, P., and Onasch, T.B.: Absorption Enhancement of Coated Absorbing Aerosols: Validation of the Photo-Acoustic Technique for Measuring the Enhancement, Aerosol Sci. Technol, 43,10, 1006-1012, doi: 10.1080/02786820903117932, 2009.

Leaitch, W.R., Macdonald, A.M., Brickell, P.C., Liggio, J., Siostedt, S.L., Vlasenko, A., Bottenheim, J.W., Huang, L., Li, S., Liu, S.K., Toom-Sauntry, D., Hayden, K.A., Sharma, S., Shantz, N.C., Wiebe, H.A., Zhang, W., Abbatt, J., Slowik, J.G., Chang, R., Russell, L.M., Schwartz, R.E., Takahama, S., Jayne, J.T., and Ng, N.: Temperature response of the

submicron organic aerosol from temperate forests, Atm. Env., 45, 6696-6704, 2011.

Levy, R.C., Remer, L. A., Kleidman, R. G., Mattoo, S., Ichoku, C., Kahn, R., and Eck, T. F.: Global evaluation of the Collection 5 MODIS dark-target aerosol products over land, Atmos. Chem. Phys., 10, 10399–10420, doi:10.5194/acp-10-10399-2010, 2010.

Li, J., Carlson, B.E., Dubovik. O., and Lacis, A.A.: Recent trends in aerosol optical properties derived from AERONET measurements, Atmos. Chem. Phys. Discuss., 14, 14351-14397, doi:10.5194/ acpd-14-14351-2014, 2014.

Liggio, J., Li, S.,Vlasenko, A., Siostedt, S.L.,Chang, R., Shantz, N., Abbatt, J., Slowik, J.G., Bottenheim, J.W., Brickell, P.C., Stroud, C., and Leaitch, R.R.: Primary and secondary organic aerosols in urban air masses intercepted at a rural site, J. Geophys. Res., 115, D21305, doi: 12010JD0144260.1029/, 2010.

Link, M.F., Zhou,Y., Taubman, B.F., Sherman, J.P., Sive, B.C., Morrow,H., Krintz, I., Robertson, L., Cook, R., Stocks, J., and West, M.: A characterization of volatile organic compounds and secondary organic aerosol at a mountain site in the southeastern United States Estimating background secondary organic aerosol in the southeastern United States from a regionally representative site, J. Atmos. Chem, doi: 10.1007/s10874-015-9305-5, 2015.

Malm, W.C., Schichtel, B.A., Pitchford, M.L., Ashbaugh, L.L., and Eldred, R.A.: Spatial and monthly trends in speciated fine particle concentration in the United States. J. Geophys. Res, 109, D03306, doi: 10.1029/2003JD003739, 2004.

Müller, T., Henzing, J.S., de Leeuw, G., Wiedensohler, A., Alastuey, A., Angelov, H., Bizjak, M., Collaud Coen, M., , Engstrom, J. E. Gruening, C., Hillamo, R., Hoffer, A., Imre, K., Ivanow, P., Jennings, G., Sun, J.Y., Kalivitis, N., Karlsson, H., Komppula, M., Laj, P., Li, S-M., Lunder, C., Marinoni, A., Martins dos Santos, S., Moerman, M., Nowak, A., Ogren, J.A., Petzold, A., Pichon, J.M., Rodriquez, S., Sharma, S., Sheridan, P.J., Teinila, K., Tuch, T., Viana, M., Virkkula, A., Weingartner, E., Wilhelm, R., and Wang, Y.Q.: Characterization and inter-comparison of aerosol absorption photometers: result of two inter-comparison workshops, Atmos. Meas. Tech., 4, 245–268, 2011.

Murphy, D.M., Capps, S. L., Daniel, J. S., Frost, G. J., and White, W. H.: Weekly patterns of aerosol in the United States, Atmos. Chem. Phys., 8, 2729–2739, doi:10.5194/acp-8-

2729-2008, 2008.

Murphy, D.M., Chow, J.C., Leibensperger, E.M., Malm, W.C., Pitchford, M., Schichtel, B.A., Watson, J.G., and White, W.H.: Decreases in elemental carbon and fine particle mass in the United States, Atmos. Chem. Phys., 11, 4679–4686, doi:10.5194/acp-11-4679-2011, 2011.

Ogren, J. A.: Comment on "Calibration and Intercomparison of Filter-Based Measurements of Visible Light Absorption by Aerosols", Aerosol Sci. Technol., 44, 589-591, doi:10.1080/02786826.2010.482111, 2010.

Ogren, J.A., Wendell, J. Sheridan, P.J., Hageman, D., and Jefferson, A.: Continuous light absorption photometer performance, ASR Science Team Meeting, Potomac, Md, USA, March 18-21, 2013, available at http://asr.science.energy.gov/meetings/stm/posters/view?id=781, last access: 26 October 2014.

Parworth C., Fast, J, Mei, F., Shippert, T., Sivaraman, C., Tilp, A.,Watson, T., and Zhang, Q.: Long- term measurements of sub-micrometer aerosol chemistry at the Southern Great Plains (SGP) using an aerosol chemical speciation monitor (ACSM), Atm. Env., 106, 43-55, 2015.

Quinn, P. K., Bates, T. S., Baynard, T., Clarke, A. D., Onasch, T. B., Wang, W., Rood, M., Andrews, E., Allan, J., Carrico, C. M., Coffman, D., and Worsnop, D.: Impact of particulate organic matter on the relative humidity dependence of light scattering: A simplified parameterization, Geophys. Res. Lett., 32(L22809), doi:101029/2005GL024322, 2005.

Rupakheti, M., Leaitch, R., Lohmann, U., Hayden, K., Brickell, P., Lu, G., Li, S., Toom-Sauntry D., Bottenheim, J.W., Brook, J.R., Vet, R., Jayne, J.T., and Worsnop, D.R.: An Intensive Study of the Size and Composition of Submicron Atmospheric Aerosols at a Rural Site in Ontario, Canada, Aerosol Science and Technology, 39:8, 722-736, DOI: 10.1080/02786820500182420, 2005.

Schuster, G.L., Dubovik, O., and Holben, B.N.: Angstrom exponent and bimodal aerosol size distributions, J. Geophys. Res., 111, D07207, doi:10.1029/2005JD006328, 2006.

1631 Seinfeld, J. H. and Pandis, S. N.: Atmospheric chemistry and physics: from air pollution to
1632 climate change, 2nd edition, John Wiley & Sons, New York, New York, USA, 1998.

1633 Sheridan, P. J., and Ogren, J. A.: Observations of the vertical and regional variability of aerosol
1634 optical properties over central and eastern North America, J. Geophys. Res., 104, D14, 16793-
1635 16805, doi:10.1029/1999JD900241, 1999.

1636 Sheridan, P. J., Delene, D. J., and Ogren, J. A.: Four years of continuous surface
1637 aerosol measurements from the Department of Energy's Atmospheric Radiation Measurement
1638 Program Southern Great Plains Cloud and Radiation Testbed site, J. Geophys. Res.,
1639 106, D18, 20735-20747, doi:10.1029/2001JD000785, 2001.

1640 Sheridan, P. J., Jefferson, A., and Ogren, J. A.: Spatial variability of submicrometer
1641 aerosol radiative properties over the Indian Ocean during INDOEX, J. Geophys. Res., 107,
1642 D19, 8011, doi:10.1029/2000JD000166, 2002.

1643 Sheridan, P. J., Andrews, E., Ogren, J. A., Tackett, J. L., and Winker, D. M.: Vertical
1644 profiles of aerosol optical properties over central Illinois and comparison with surface and
1645 satellite measurements, Atmos. Chem. Phys., 12, 11695–11721, doi:10.5194/acp-1 2-11695-
1646 2012, 2012.

1647 Slowik, J. G., Stroud, C., Bottenheim, J. W., Brickell, P. C., Chang, R. Y.-W., Liggio, J.,
1648 Makar, P. A., Martin, R. V., Moran, M. D., Shantz, N. C., Sjostedt, S. J., van Donkelaar, A.,
1649 Vlasenko, A., Wiebe, H. A., Xia, A. G., Zhang, J., Leaitch, W. R., and Abbatt, J. P. D.:
1650 Characterization of a large biogenic secondary organic aerosol event from eastern
1651 Canadian forests, Atmos. Chem. Phys., 10, 2825–2845, doi:10.5194/acp-10-2825-2010,
1652 2010.

1653 Spak, S.N and Holloway, T.: Seasonality of speciated aerosol transport over the Great Lakes
1654 region, J. Geophys. Res., 114, D08302, doi:10.1029/2008JD010598, 2009.

1655 US Census Bureau. 2010. 2006–2010 American Community Survey. Available at
1656 http://www.census.gov/acs/www/, Accessed January 3, 2012.

1657 van de Hulst, H.C.: Light scattering by small particles, John Wiley and Sons, New York, 1957.

1658 Wiscombe, W. J. and Grams, G. W.: The backscattered fraction in two-stream approximations,
1659 J. Atmos. Sciences, 33, 2440-2451, 1976.

WMO: WMO/GAW Aerosol Measurement procedures guidelines and recommendations. World Meteorological Organization, Technical Document No. 1178, GAW Report No. 153, 2003.

Yang, F., Huang, L., Sharma, S., Brook, J.R., Zhang, W., Li, S., and Tan, J.: Two-year observations of fine carbonaceous particles in variable sampling intervals, Atm. Env., 45, 2418-2426, 2011.

Yoon, J., von Hoyningen-Huene, W., Kokhanovsky. A.A., Vountas M., and Burrows. J.P.: Trend analysis of aerosol optical thickness and Ångström exponent derived from the global AERONET spectral observations, Atmos. Meas. Tech., 5, 1271–1299, doi:10.5194/amt-5-1271-2012, 2012.

Yu, H., Kaufman, Y., Chin, M., Feingold, G., Remer, L., Anderson, T., Balkanski, Y., Bellouin,N., Boucher, O., Christopher, S., DeCola,P., Kahn,R., Koch, D., Loeb, N., Reddy, M. S., Schulz,, M., Takemura, T., and Zhou,M.: A review of measurement-based assessments of aerosol direct radiative effect and forcing, Atmos. Chem. Phys., 6, 613-666. 2006.

Yu, H., Quinn, P.K., Feingold, G., Remer, L.A., Kahn, R.A., Chin, M., and Schwartz, S.E.: Remote Sensing and *In Situ* Measurements of Aerosol Properties, Burdens, and Radiative Forcing, in Atmospheric Aerosol Properties and Climate Impacts, A Report by the US Climate Change Science Program and the Subcommittee on Global Change Research. [Mian Chin, Ralph A. Kahn, and Stephen E. Schwartz (eds.)], National Aeronautics and Space Administration, Washington, D.C., USA, 2009.

Zhang, X, Hecobian, A., Zheng, M., Frank, N. H., and Weber, R. J.: Biomass burning impact on PM2.5 over the southeastern US during 2007: integrating chemically speciated FRM filter measurements, MODIS fire counts and PMF analysis, Atmos. Chem. Phys., 10, 6839–6853, doi:10.5194/acp-10-6839-2010, 2010.

Table 1. Sites, instruments and data period included in the study, listed from west to east. Aerosol sampling size cuts and the instrument used to measure absorption is also included. All sites used a TSI 3563 3-λ nephelometer[1] to measure total scattering and hemispheric backscattering

Site	Lat/Long (deg)	Elev.(m) asl	Yrs data used	# Hrs used 2010-2013	Size cut (μm)	Absorption instrument (dates used mm/yy)
SGP	36.6N, 97.5W	315	1997-2013[5]	32,971(σ_{sp}) 25,140(σ_{ap})	1,10	3-λ PSAP[3] (1/10-12/13)
BND	40.0N, 88.4W	230	1996-2013	33,449(σ_{sp}) 32,040(σ_{ap})	1,10	1-λ PSAP[2] (9/96-2/06) 3-λ PSAP (3/06-2/12) 3-λ CLAP[4] (3/12-12/13)
EGB	44.2N, 79.8W	253	2010-2013	32,448(σ_{sp}) 26,304(σ_{ap})		1-λ PSAP (1/10-12/13
APP	36.2N, 81.7W	1080	2010-2013	34,220(σ_{sp}) 34,178(σ_{ap})	1,10	3-λ PSAP (1/10-12/13)

[1]3-λ TSI nephelometer measures at λ=450, 550,700 nm; [2]1-λ PSAP measures at 565 nm, adjusted to 550 nm using Bond et al. (1999) correction; [3]3-λ PSAP measures at 467, 530, 660 nm; [4]3-λ CLAP measures at 467, 529, 653 nm; [5] SGP aerosol light scattering data from 1997-2013 is used but absorption data is only used from 2010-2013.

Table 2. Parameters and equations used to calculate aerosol optical properties. Constants and parameters used in the formula to calculate globally-averaged top-of-atmosphere direct radiative forcing (DRFE) for each site are also included and are denoted with **.

Parameter	**Equation (or value)**
Extinction Coefficient	$\sigma_{ep}=\sigma_{sp}+\sigma_{ap}$
Single-scattering albedo	$\omega_{0}=\sigma_{sp} / \sigma_{ep} = \sigma_{sp} / (\sigma_{sp}+\sigma_{ap})$
Hemispheric backscatter fraction	$b = \sigma_{bsp} / \sigma_{sp}$
Scattering Ångström exponent	$\alpha_{sp} = -\log(\sigma_{sp}(\lambda_1) / \sigma_{sp}(\lambda_2)) / \log(\lambda_1 / \lambda_2)$
Absorption Ångström exponent	$\alpha_{ap} = -\log(\sigma_{ap}(\lambda_1) / \sigma_{ap}(\lambda_2)) / \log(\lambda_1 / \lambda_2)$
Sub-micron scattering fraction	$R_{sp}= \sigma_{sp,1} / \sigma_{sp,10}$
Sub-micron absorption fraction	$R_{ap}= \sigma_{ap,1} / \sigma_{ap,10}$
Direct Radiative Forcing Efficiency	$DRFE=DRF/AOD= -D\, S_0\, T^2_{atm}\, (1-A_c)\, \beta\, \omega_0 * [\, (1-R_s)^2 - (2\, R_s / \omega_0\, \beta)\, (1-\omega_0)\,]$
Upscatter Fraction**	$\beta= 0.0817 +1.8495*b -2.9682*b^2$
Fractional Day Length**	D=0.50 (globally-averaged)
Solar Constant**	$S_0=1370$ W m^{-2}
Atmospheric Transmission**	$T_{atm}=0.76$ (globally-averaged)
Cloud Fraction**	$A_c=0.60$ (globally-averaged)
Spectrally-averaged surface albedo**	$R_s=0.15$ (globally-averaged)

Table 3. Total and precision fractional uncertainties (%) of measured aerosol optical properties (AOPs) σ_{sp}, σ_{bsp}, and σ_{ap} and calculated AOPs (e.g., the intensive AOPs) for 1-hour averaging time. Uncertainties are expressed as 95% confidence intervals. All calculated uncertainties are for λ=550 nm except for α_{sp} and α_{ap}, which are calculated for the 450/700 nm wavelength pair. All AOPs are PM1 except for PM10 α_{sp} and the PM1 scattering and absorption fractions (R_{sp} and R_{ap}, respectively). The uncertainties in columns 3 and 4 differ only by inclusion of the PSAP unit-to-unit variability term (Eq. S3) in column 3. All uncertainties except $\Delta\sigma_{sp}$, $\Delta\sigma_{bsp}$, and $\Delta\sigma_{ap}$ depend nonlinearly on the measured value, and cannot rigorously be represented as a percentage[1]. For these intensive AOP uncertainties, we use approximate annual-mean values $\sigma_{sp,10}$=30 Mm^{-1}, $\sigma_{ap,10}$=3.0 Mm^{-1}, R_{sp}=0.80, R_{ap}=0.88, b=0.14, ω_0=0.91, α_{sp}=2.0, and α_{ap}=1.0 to calculate fractional uncertainties. The intensive AOP fractional uncertainties apply for the average conditions listed above, and the equations in the Supplementary Materials to this manuscript should be used to calculate uncertainties at different sites or for different conditions.

	Total uncertainty %	Precision uncertainty % for comparisons among sites	Precision uncertainty % for comparisons at single site
$\Delta\sigma_{sp}$	8.0	3.8	3.8
$\Delta\sigma_{bsp}$	8.1	4.0	4.0
$\Delta\sigma_{ap}$	20	20	12
ΔR_{sp}	2.7	1.1	1.1
ΔR_{ap}	4.2	4.2	2.5
Δb	2.3	1.1	1.1
$\Delta\ \omega_0$	1.5	1.7	0.9
$\Delta\ \alpha_{sp}$ (PM10)	1.8	1.4	1.4
$\Delta\ \alpha_{ap}$	17	17	10
ΔDRFE	4.8	5.2	4.8

[1]The uncertainties $\Delta\sigma_{sp}$, $\Delta\sigma_{bsp}$, and $\Delta\sigma_{ap}$ depend very weakly on measured values, through the noise term. This term represents a negligible contribution to the uncertainty for averaging times of 1 hour or more.

Table 4. Mann-Kendall slopes (%/decade) and trend significance[1] for long-term trends in several PM10 and PM1 aerosol optical properties measured at BND and SGP. Monthly-averaged data is used for the calculations. BND data for the time period 1996-2013 is used; SGP data for the time period 1997-2013 is used. Trends that are significant at or above the $p<0.05$ level are in bold.

	BND slope (%/10yr), significance	SGP Slope (%/10yr), significance
$\sigma_{sp,10}$	**-16.3, p<0.01**	**-19.6, p<0.001**
$\sigma_{sp,1}$	**-23.1, p<0.001**	**-24.0, p<0.001**
$\sigma_{ap,10}$	-15.2, not significant	N/A
$\sigma_{ap,1}$	-10.5, p<0.1	N/A
$\alpha_{sp,10}$	1.9, not significant	**-5.3, p<0.05**
b_{10}	**7.6, p<0.001**	**11.2, p<0.001**
b_1	**11.8, p<0.001**	**15.1, p<0.001**
R_{sp}	**-8.1, p<0.001**	**-9.1, p<0.001**
$\omega_{0,10}$	-0.5, not significant	N/A
$\omega_{0,1}$	**-1.55, p<0.01**	N/A

[1]Slopes and significance were obtained using the function 'TheilSen' in the R package 'openair' (Carslaw et al., 2012, Carslaw, 2015). Data were de-seasonalized and autocorrelation was accounted for using options supplied with the TheilSen function. Decadal slopes (%/10year) were calculated by multiplying the yearly slope by 10, i.e., 10*%/year.

Figure 1. Locations of the four NOAA-ESRL sites in this study- Southern Great Plains, OK (SGP); Bondville, IL (BND); Appalachian State (APP) in Boone, NC; and Egbert, Ontario, Canada (EGB).

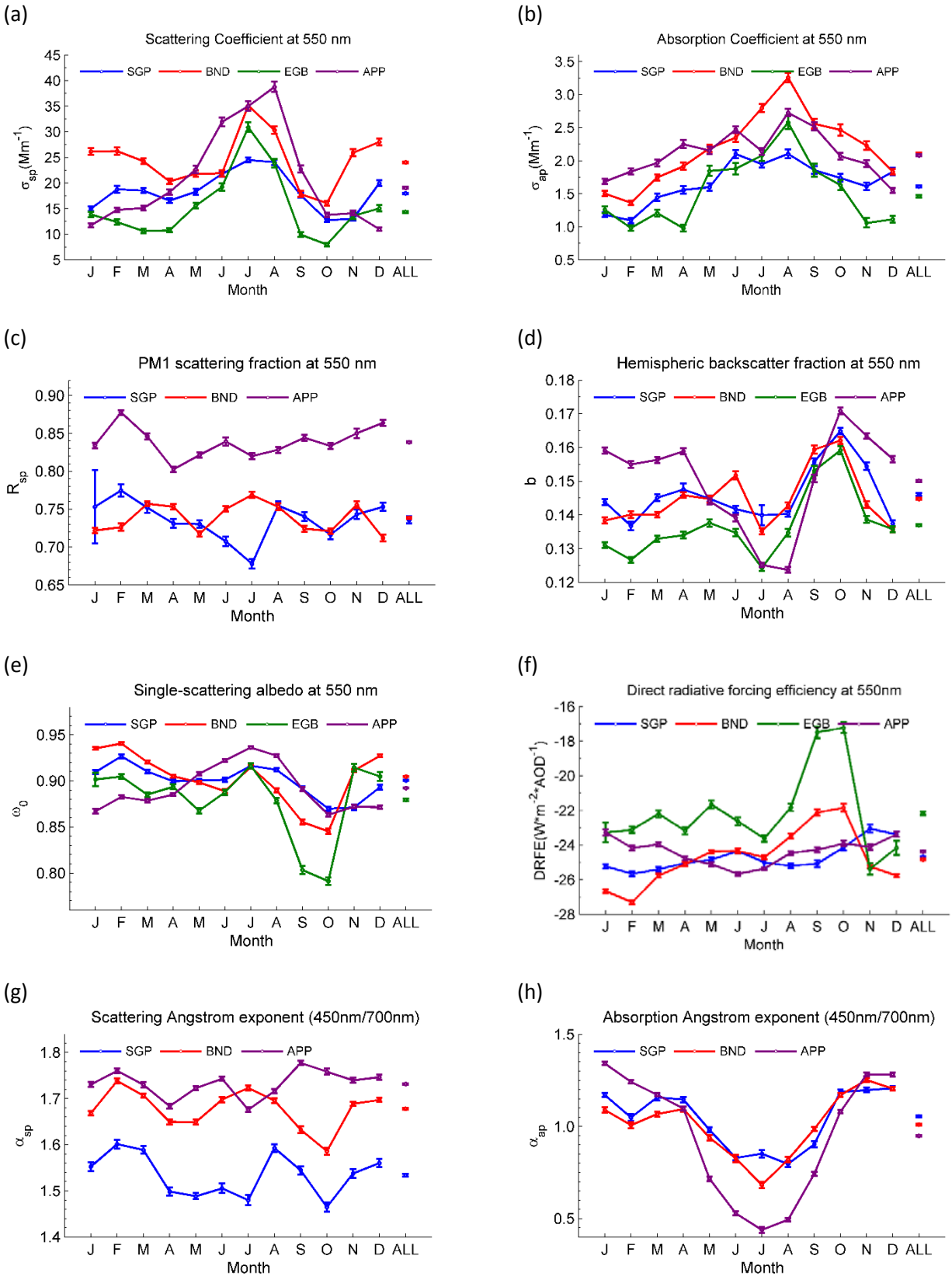

Figure 2. Annual cycle of (a) geometric mean PM1 σ_{sp} ; (b) geometric mean PM1 σ_{ap} ; (c) mean R_{sp} ; (d) mean PM1 b; (e) mean PM1 ω_0 ; (f) mean PM1 DRFE; (g) mean PM10 α_{sp} (450/700 nm); and (h) mean PM1 α_{sp} 450/700 nm) at APP, BND, EGB, and SGP over the 2010-2013 period. The values corresponding to 'ALL' are geometric mean or mean values for the entire 2010-2013 period (all months). Error bars represent 95% confidence intervals of the mean values.

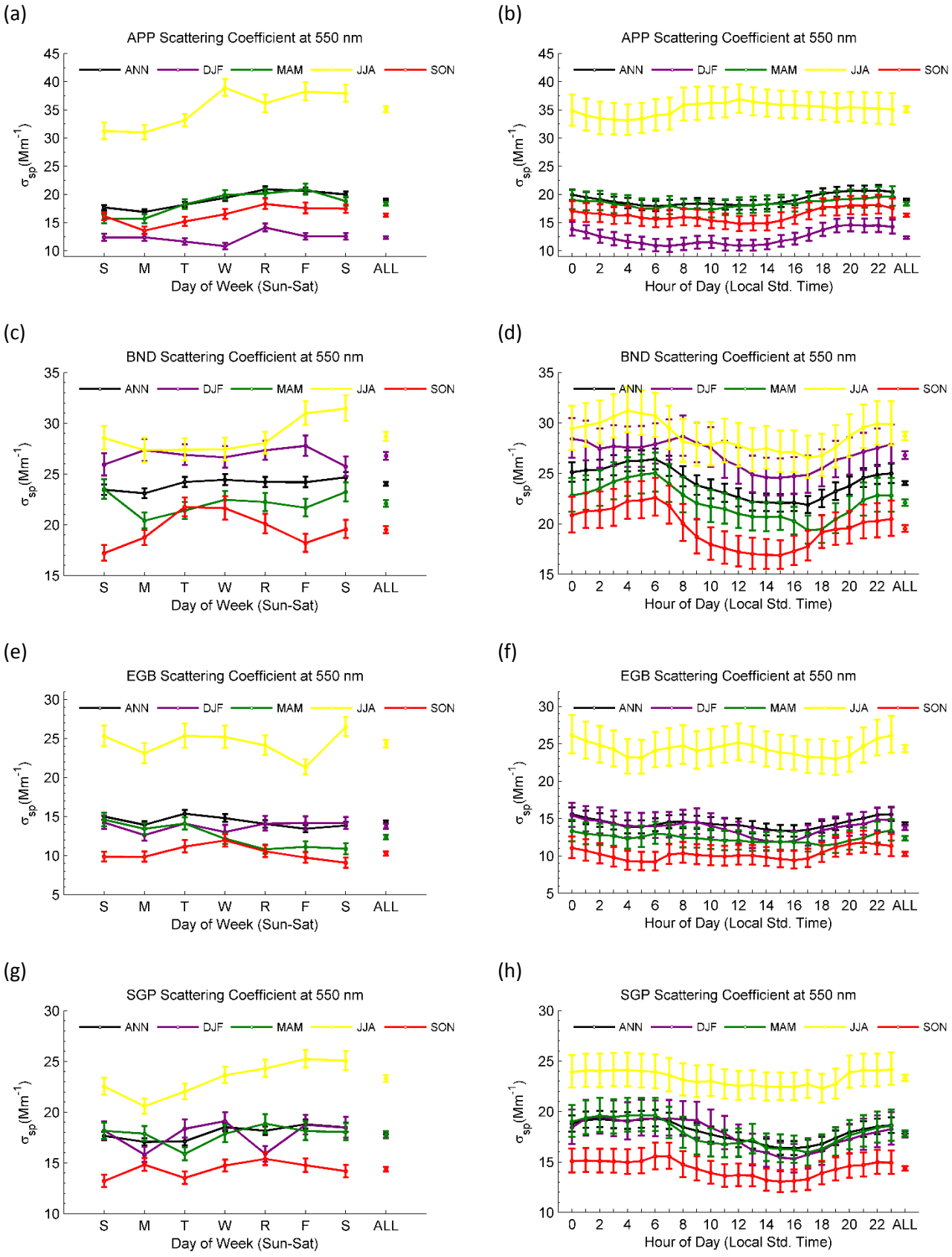

Figure 3. Weekly and diurnal cycles of geometric mean PM1 σ_{sp} over full years (ANN traces) and for winter (DJF), spring (MAM), summer (JJA), and fall (SON) at APP, BND, EGB, and SGP over the 2010-2013 period. The value corresponding to the 'ALL' data point of each trace is the mean value over all days of week or over all hours of day. Error bars represent 95% confidence intervals of mean σ_{sp} values.

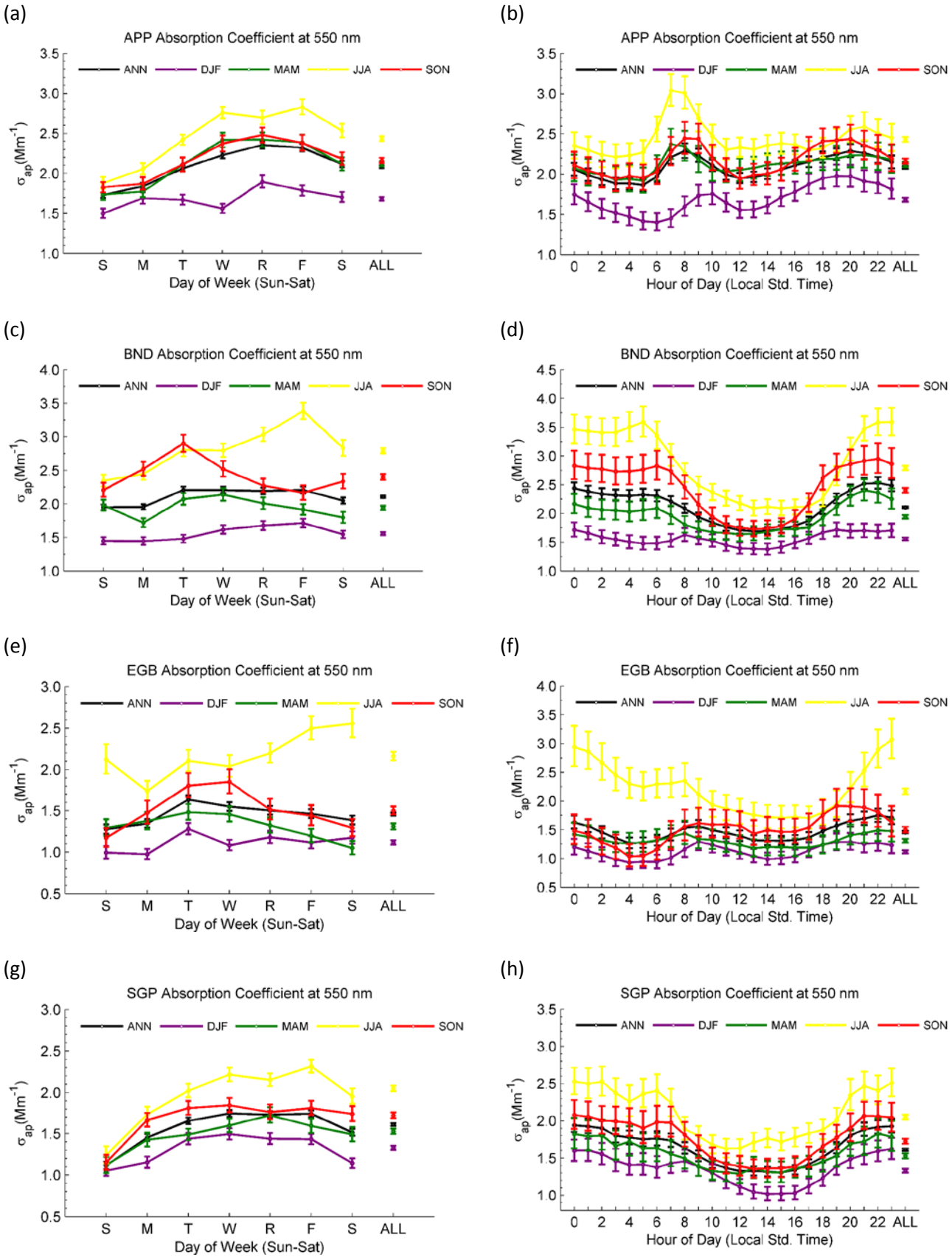

Figure 4. Weekly and diurnal cycles of geometric mean PM1 σ_{ap} over full years (ANN traces) and for individual seasons at APP, BND, EGB, and SGP over the 2010-2013 period. The value corresponding to the 'ALL' data point is the mean value over all days of week or over all hours of day. Error bars represent 95% confidence intervals of the mean values.

(a)

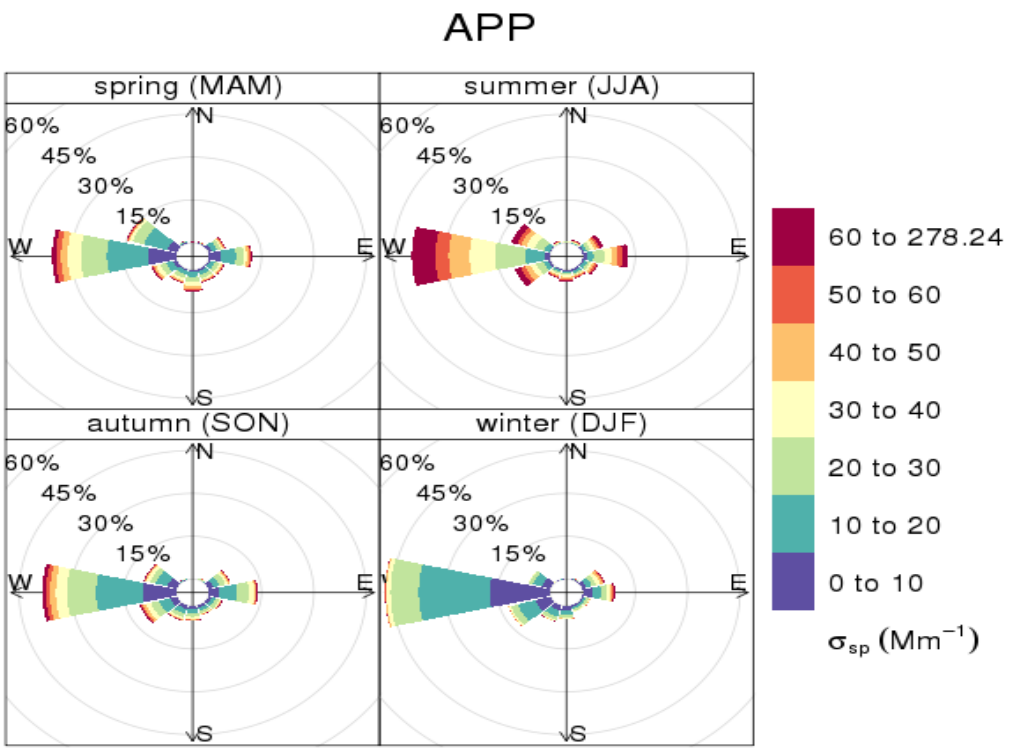

(b)

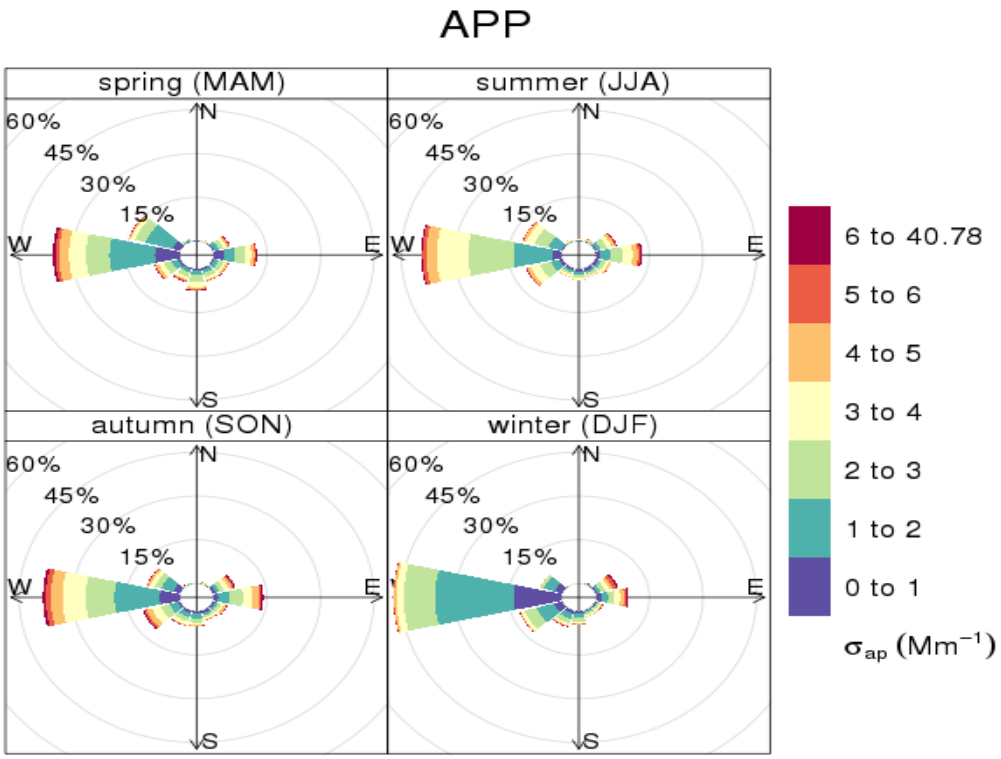

Figure 5. Pollution rose diagrams of σ_{sp} and σ_{ap} for individual seasons at APP over the 2010-2013 period. The percentages at a given radius represent the percentage of hourly profiles for a given wind sector.

(a)

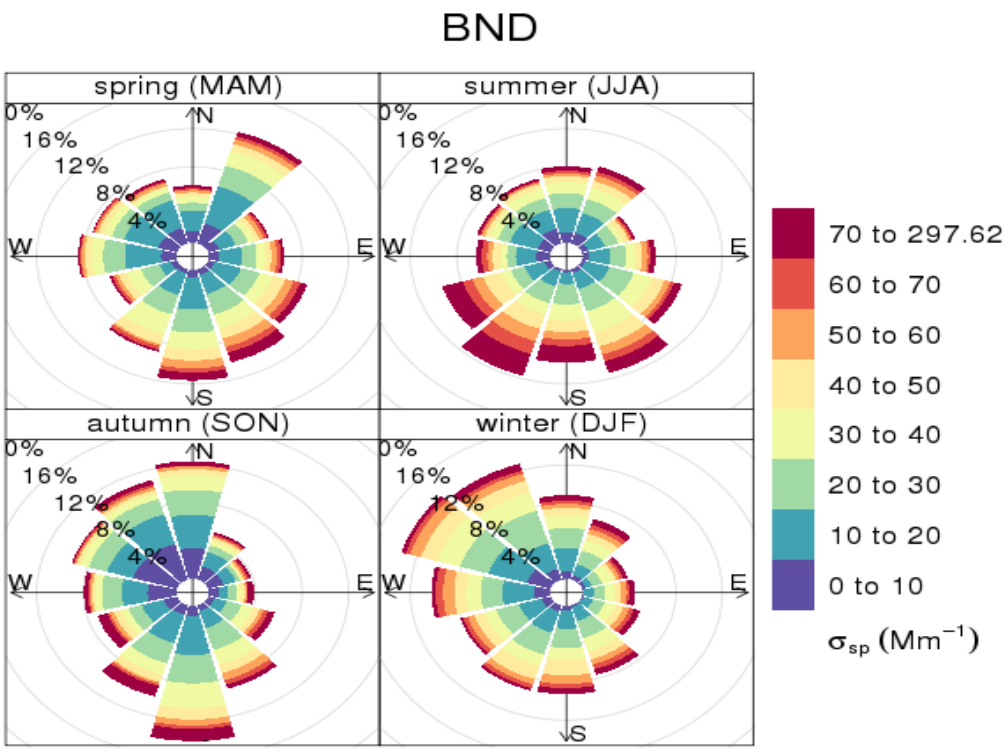

(b)

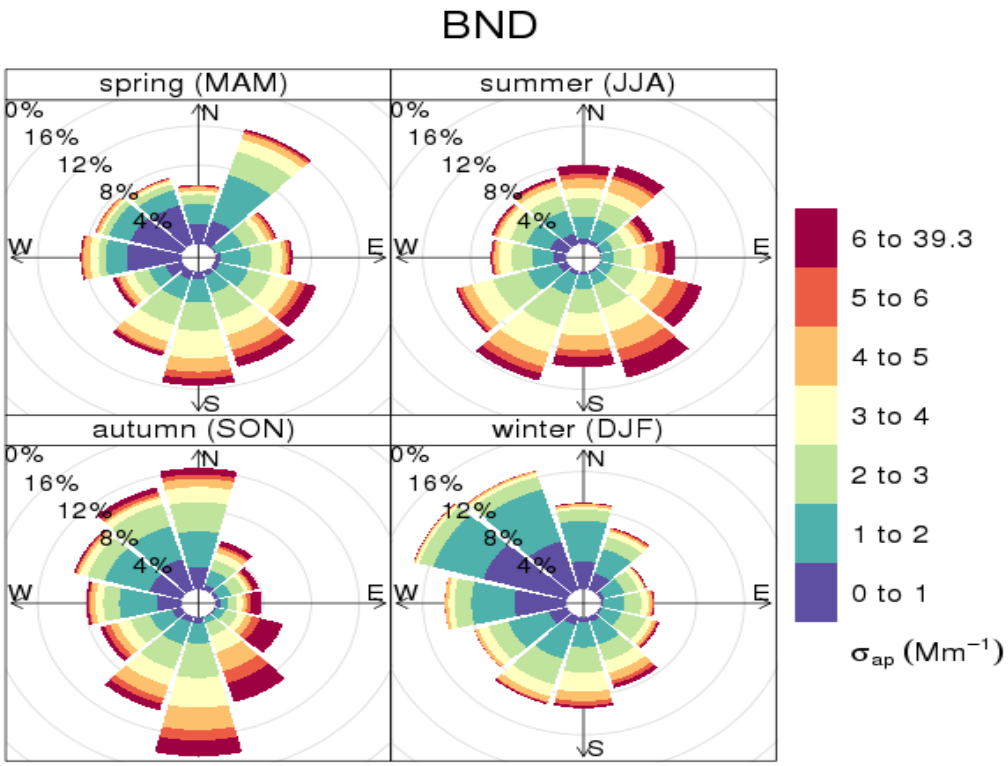

Figure 6. Pollution rose diagrams of σ_{sp} and σ_{ap} for individual seasons at BND over the 2010-2013 period. The percentages at a given radius represent the percentage of hourly profiles for a given wind sector.

(a)

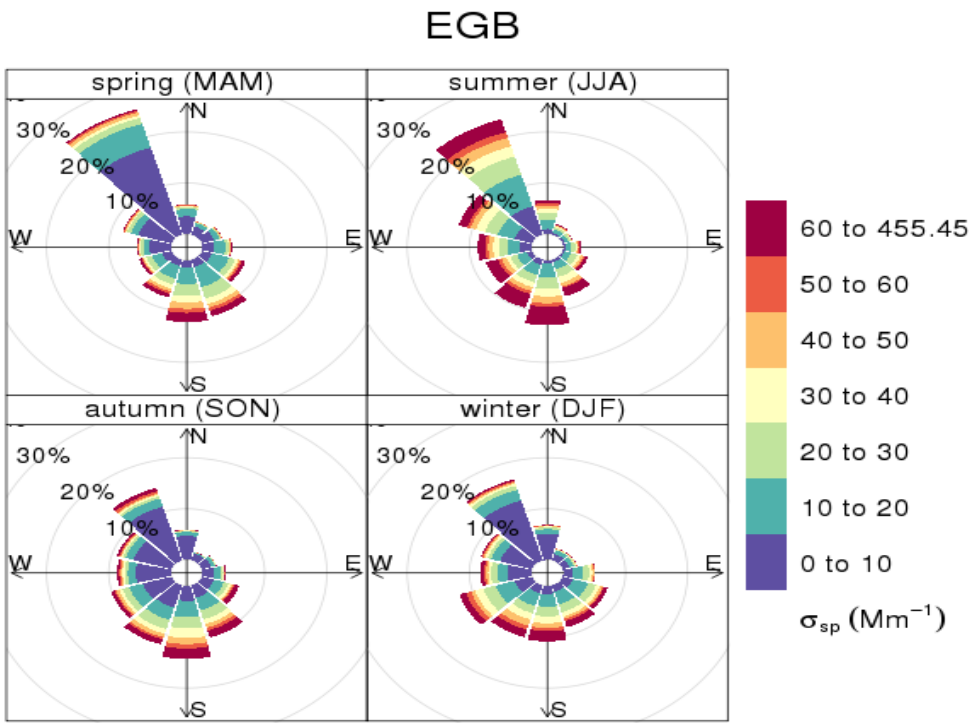

(b)

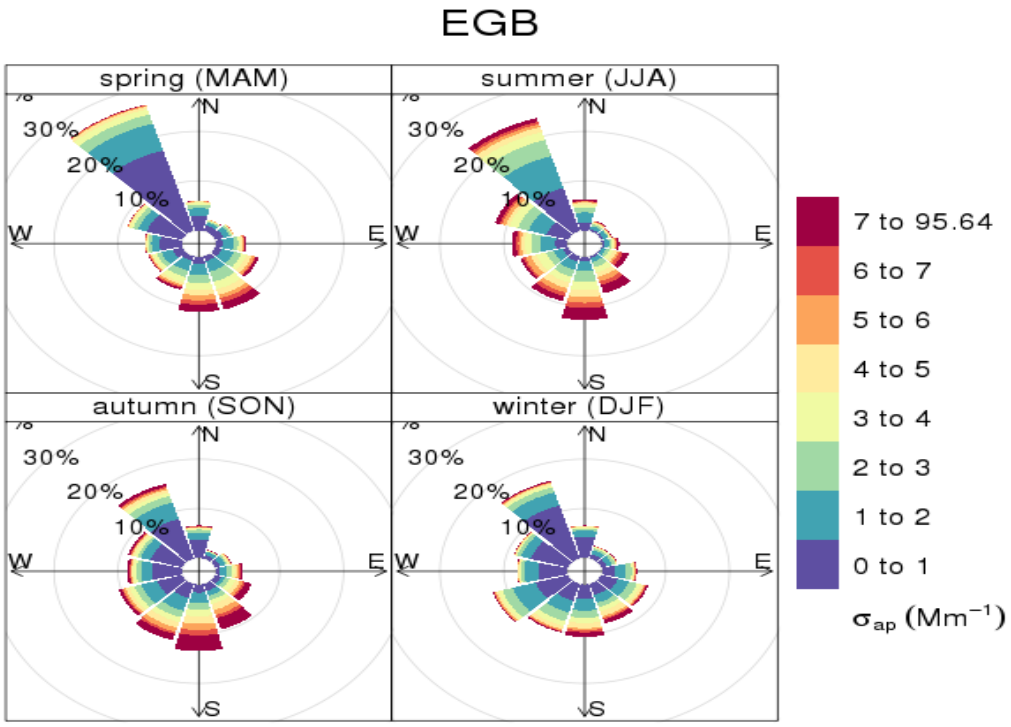

Figure 7. Pollution rose diagrams of σ_{sp} and σ_{ap} for individual seasons at EGB over the 2010-2013 period. The percentages at a given radius represent the percentage of hourly profiles for a given wind sector.

(a)

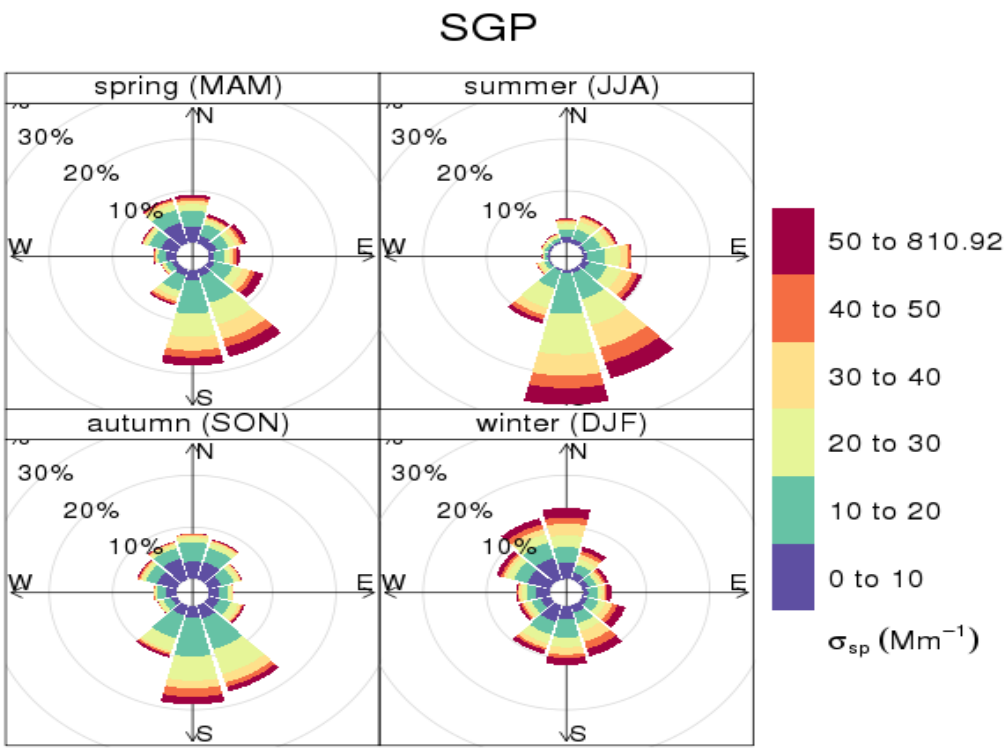

(b)

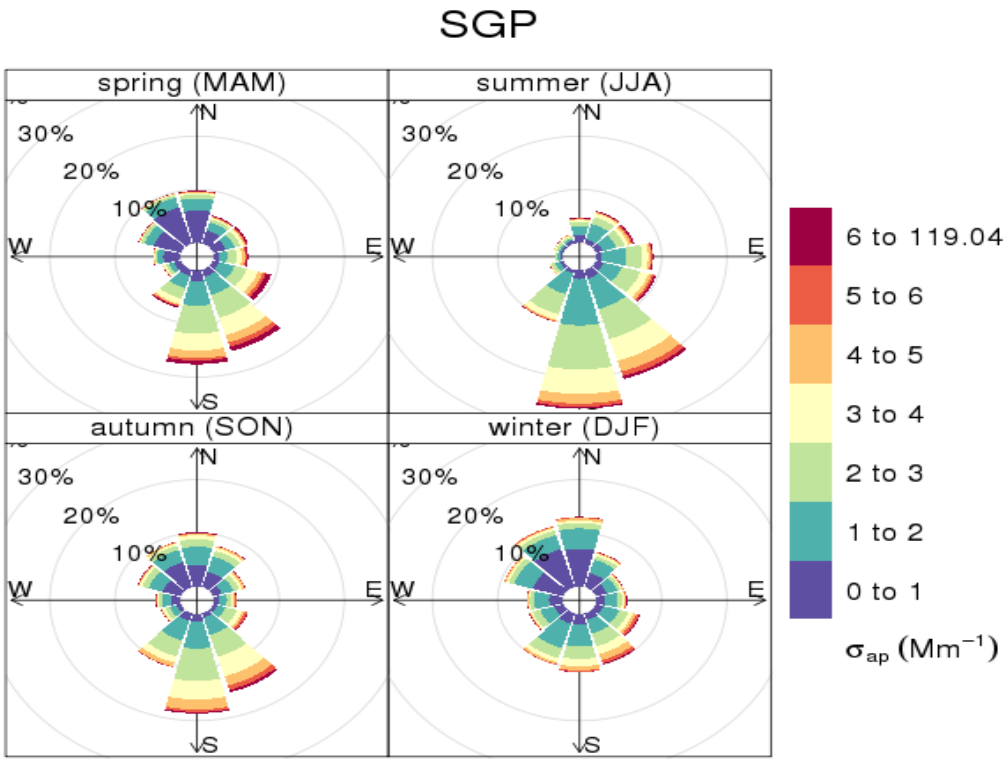

Figure 8. Pollution rose diagrams of σ_{sp} and σ_{ap} for individual seasons at SGP over the 2010-2013 period. The percentages at a given radius represent the percentage of hourly profiles for a given wind sector.

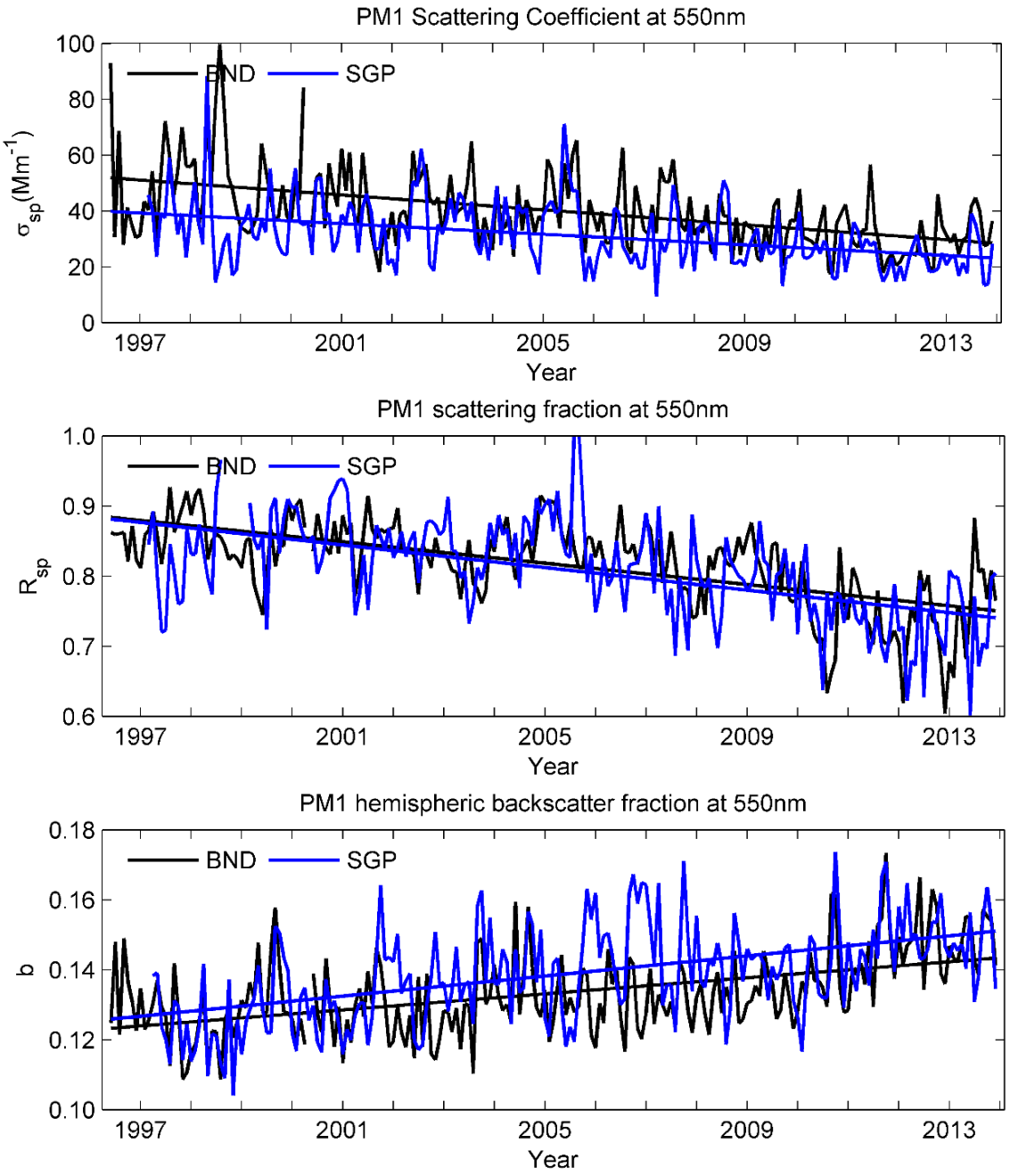

Figure 9. Time series of monthly-averaged PM1 σ_{sp}, R_{sp}, and b at 550 nm for BND (1996-2013) and SGP (1997-2013). Trend lines, representing least-squared fits of the data, are also shown.

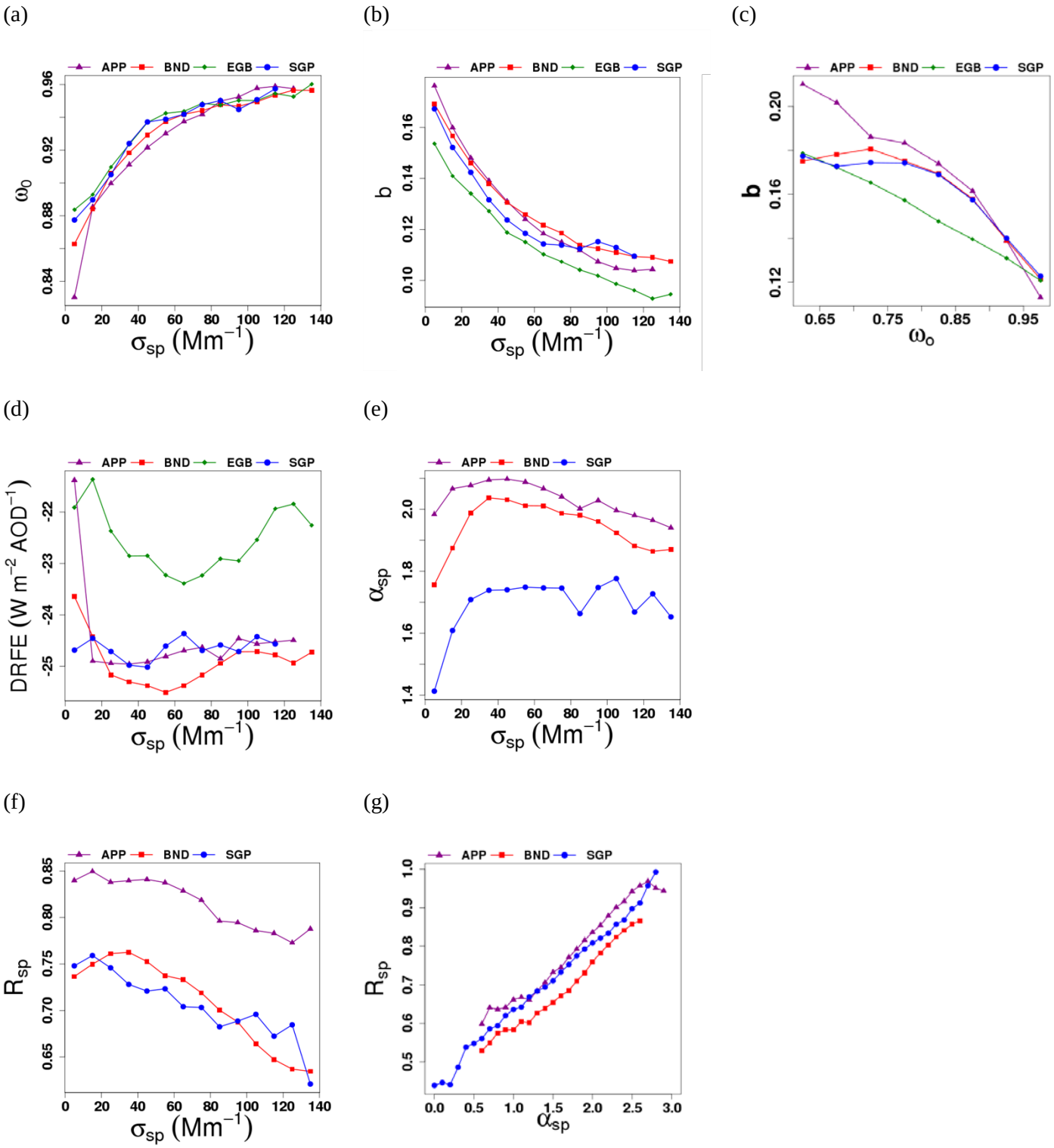

Figure 10. Systematic relationships among mean AOPs over full annual cycles of the 2010-2013 period at APP, BND, EGB, and SGP: (a) PM1 ω_0 versus PM1 σ_{sp}; (b) PM1 b versus PM1 σ_{sp}; (d) PM1 b versus PM1 ω_0; (d) PM1 DRFE versus PM1 σ_{sp}; (e) PM10 α_{sp} versus PM1 σ_{sp}; (f) R_{sp} versus PM1 σ_{sp} ; and (g) R_{sp} versus PM10 α_{sp}

.

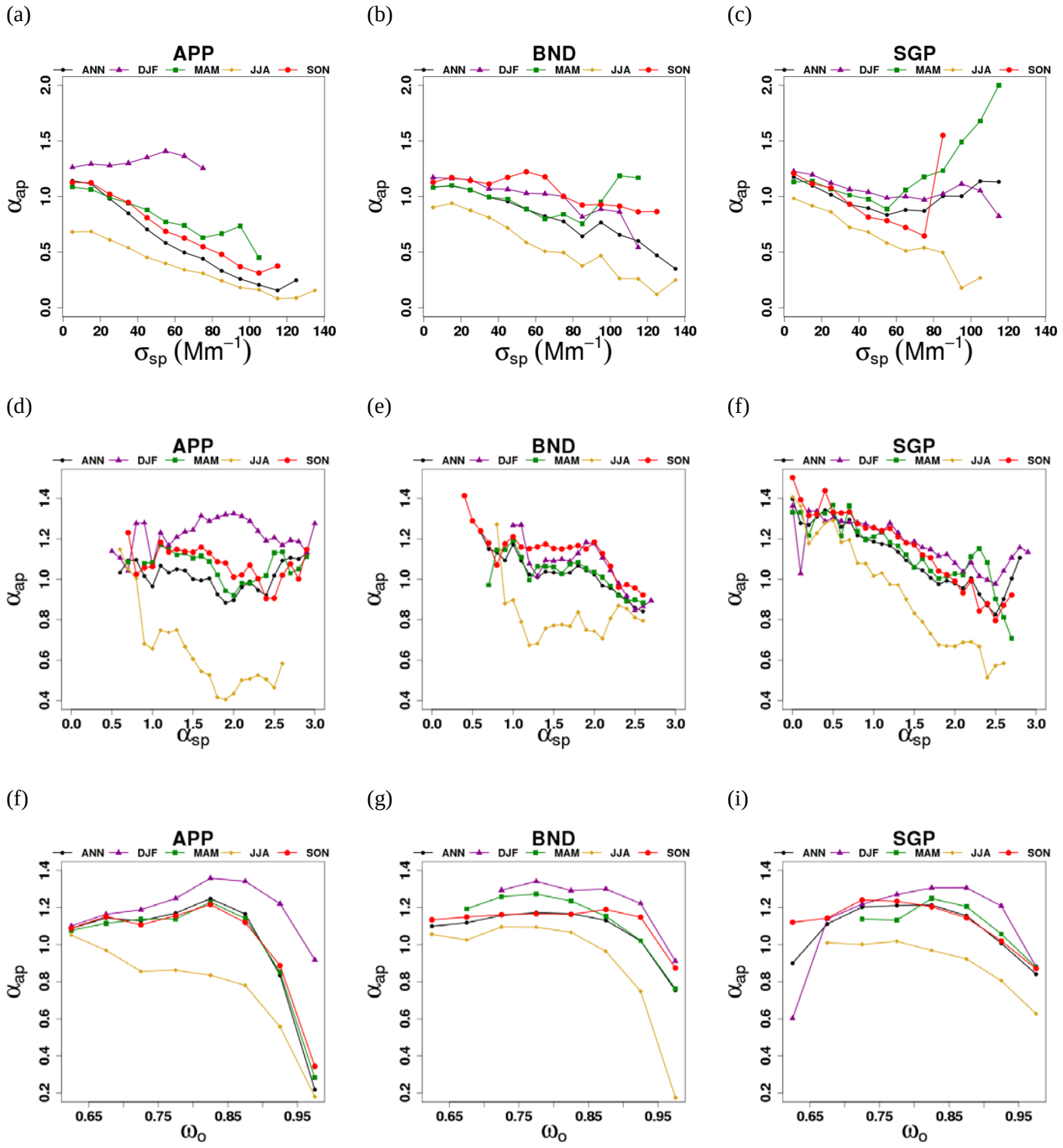

Figure 11. Systematic relationships among mean AOPs involving absorption Ångström exponent (α_{ap}) for individual seasons of the 2010-2013 period at APP, BND, and SGP: (a) α_{ap} versus σ_{sp} at APP; (b) α_{ap} versus σ_{sp} at BND; (c) α_{ap} versus σ_{sp} at SGP; (d) α_{ap} versus α_{sp} at APP; (e) α_{ap} versus α_{sp} at BND; (f) α_{ap} versus α_{sp} at SGP; (g) α_{ap} versus ω_0 at APP; (h) α_{ap} versus ω_0 at BND; (i) α_{ap} versus ω_0 at SGP.